Gondwana Research 85 (2020) 55–75

Contents lists available at ScienceDirect

Gondwana Research

journal homepage: www.elsevier.com/locate/gr

2.8–1.7 Ga history of the Jiao-Liao-Ji Belt of the North China Craton from the geochronology and geochemistry of mafic Liaohe meta-igneous rocks

Kaj Hoernle [a,b,*], Bruce Schaefer [c], Sanzhong Li [d], Folkmar Hauff [a], Xiyao Li [d], Dieter Garbe-Schönberg [b], Ruixin Zhang [d], Yiming Liu [d]

[a] GEOMAR Helmholtz Centre for Ocean Research Kiel, Wischhofstr. 1-3, 24148 Kiel, Germany
[b] Institute of Geosciences, Kiel University, Kiel, Germany
[c] Earth and Planetary Sciences, Macquarie University, NSW 2109, Australia
[d] Department of Marine Geology, Ocean University of China, 266003 Qingdao, China

ARTICLE INFO

Article history:
Received 4 December 2019
Received in revised form 24 March 2020
Accepted 31 March 2020
Available online 22 May 2020

Handling Editor: M. Santosh

Keywords:
Liaohe Group
Jiao-Liao-Ji Belt
North China Craton
Neoarchean to Paleoproterozoic
Rb-Sr
Sm-Nd
Lu-Hf
U-Th-Pb isotope ages
major and trace element geochemistry
Subduction zone magmatism

ABSTRACT

The assembly and long-term evolution of the Eastern Block of the North China Craton are poorly constrained. Here we use bulk rock geochronological and geochemical data from mafic meta-igneous rocks (hornblendites, amphibolites and a metagabbro) of the Liaohe Group to reconstruct the Neoarchean to Paleoproterozoic history of the Jiao-Liao-Ji Belt, located between the Longgang and Nangrim blocks that together form the Eastern Block of the North China Craton. The mafic/ultramafic meta-igneous rocks have intrusive or tectonic contacts with the Liaoji granitic rocks (~2.2–2.0 Ga), which form the basement of the Jiao-Liao-Ji Belt. The major and trace element data indicate that the protoliths had calc-alkaline composition and formed along an active continental margin subduction zone. The mafic rocks form a whole-rock $^{176}Lu/^{177}Hf$ isochron with an age of 2.25 ± 0.31 Ga, overlapping with U—Pb zircon ages for mafic and granitic rocks from the Jiao-Liao-Ji Belt and consistent with being the emplacement age of the mafic protoliths along the active continental margin. In contrast, the whole-rock $^{147}Sm/^{144}Nd$ isochron age of 2.83 ± 0.18 Ga is likely to reflect the average age of the lithospheric mantle source from which the mafic/ultramafic protoliths were extracted. Together with geological evidence, we propose that the southwestern portion of the Longgang Block was an active continental margin since at least the early Paleoproteorozic. Literature age data from metamorphic zircons show that peak granulite metamorphism took place at ~1.96–1.88 Ga, resulting from the collisional event that fused the Longgang and Nangrim blocks into the Eastern Block of the North China Craton. Our bulk-rock $^{207}Pb/^{206}Pb$ age of 1824 ± 19 Ma and our $^{87}Rb/^{86}Sr$ age of 1671 ± 58 Ma reflect retrograde (cooling) stages during the exhumation of the Jiao-Liao-Ji Belt after the orogenesis.

1. Introduction

Archean to Palaeoproterozoic terranes record protracted periods of crustal formation, lithospheric stabilization, subsequent orogenesis and early history of plate tectonics. The inevitably poly-deformed nature of the oldest cratonic regions on Earth requires multiple geochemical and geochronological tools in order to unravel the complete and complex history of lithospheric formation, stabilization, crustal differentiation and subsequent reworking through subduction and orogenesis. Zircon geochronology employing U—Pb and Lu—Hf isotope systems has emerged as the most widely used tool for tracing parts of these processes; however, information derived from such studies is through necessity limited to stages of the orogenic cycle in which zircon grows or is recrystallized. This leaves significant portions of the geologic record, particularly those involving mafic rocks, underrepresented and effectively unsampled. Hence integration of complementary isotopic techniques to constrain the timing, onset and duration of processes acting upon Precambrian lithosphere is required. Critically, mafic and ultramafic rocks represent significant portions of the Precambrian record and offer links between the early crust, the mantle (both lithospheric and asthenospheric) from which it is derived, and its subsequent amalgamation into cratons (e.g. Manikyamba and Khanna, 2007; Hawkesworth et al., 2010; Naeraa et al., 2012; Zhao and Zhai, 2013).

The North China Craton is one of the oldest cratons on Earth, containing rocks ≥3.8 Ga (e.g. Liu et al., 1992; Song et al., 1996). It is subdivided into micro-continental blocks (Li et al., 2018) by three Paleoproterozoic mobile/orogenic belts: 1) the Khondalite Belt within the Western Block, 2) the Trans-North China Orogen separating the Eastern and Western Blocks and 3) the Jiao-Liao-Ji Belt (JLJB) within the Eastern Block (Fig. 1A).

* Corresponding author at: GEOMAR Helmholtz Centre for Ocean Research Kiel, Wischhofstr. 1-3, 24148 Kiel, Germany.
E-mail address: khoernle@geomar.de (K. Hoernle).

https://doi.org/10.1016/j.gr.2020.03.012

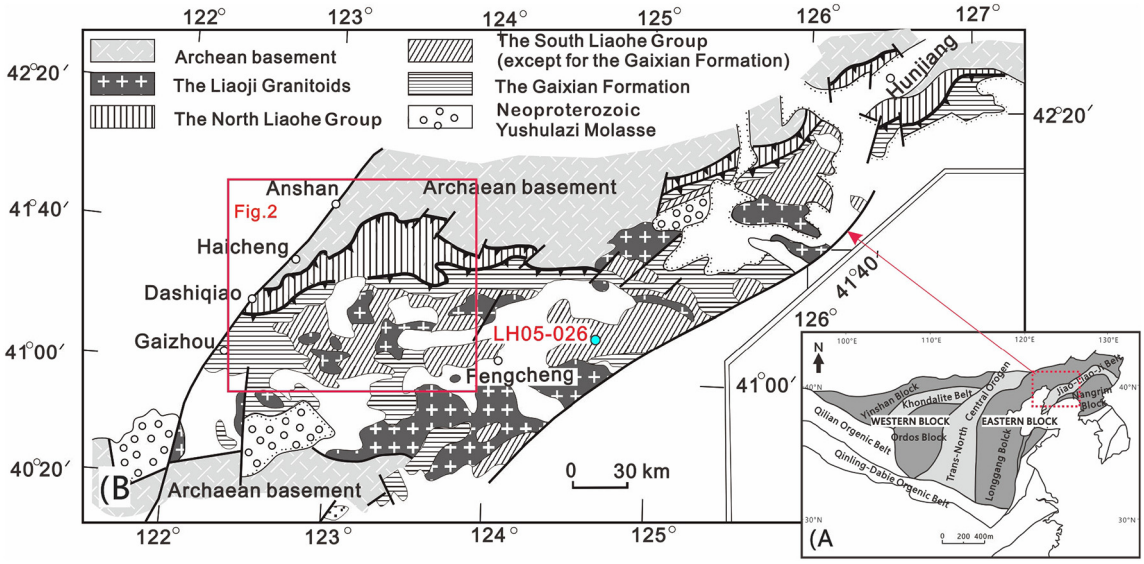

Fig. 1. A) Large-scale overview map (after Zhao et al., 2005) of the Eastern and Western blocks separated by the Trans-North China Orogen. The box shows the location of B) blow-up map (after Li et al., 2005a, 2005b) showing the Paleoproterozoic Jiao-Liao-Ji Belt (JLJB), which divides the Eastern Block into two microcontinental blocks: the Longgang (NW) and Nangrim (SE) blocks. Red box shows the location of Fig. 2. Blue circle shows South Liaohe sample location. (For interpretation of the references to colour in this figure legend, the reader is referred to the web version of this article.)

The Khondalite Belt separates the Western Block into the Yinshan (NW) and Ordos (SE) blocks and presumably formed through the collision of the two smaller blocks at ~1.95 Ga (e.g. Zhao et al., 2002a, 2002b, 2005; Xia et al., 2006; Santosh et al., 2007). The Trans-North China Orogen separates the Western and Eastern blocks and resulted through their collision and amalgamation at ~1.85 Ga (e.g. Zhao et al., 1998, 1999, 2000, 2001a, b, 2002a, b, 2003, 2004, 2005, 2006a, b, 2010, 2012, 2013; Zhai et al., 1993, 2000, 2005; Zhai and Liu, 2003; Kröner et al., 1998, 2005, 2006; Guan et al., 2002; Guo et al., 2002, 2005; Zhang et al., 2006, 2007; Zhao, 2009; Santosh, 2010; Zhai, 2011; Zhai and Santosh, 2011; Li et al., 2010, 2012; Wang et al., 2013; Santosh et al., 2013, 2015; Li and Santosh, 2018). The JLJB divides the Eastern Block into the Longgang (NW) and Liaonan-Nangrim (SE) blocks, but its origin and tectonic evolution remain controversial despite a large number of recent studies on the belt (Shen and Hu, 1986; Jiang, 1987; Zhang and Yang, 1988; Yang et al., 1988; Jahn et al., 2008; LBGMR, 1989; Wang and Yan, 1992; Liu et al., 1992; Hu, 1992; Sun et al., 1993, 1996; Cao, 1996; Yu, 1996; Liu and Li, 1996; Lu, 1996; Lu et al., 1996; Paek and Jon, 1996; Kim and Jon, 1996; Wang et al., 1997; Li and Yang, 1997; Chen et al., 2001; Li et al., 2001a, 2001b, 2005a, 2005b, Li et al., 1997a, 1997b; Li et al., 2011a, 2011b; Li and Zhao, 2007; Lin et al., 1998; Xu et al., 1998; Liu et al., 1998; Xu et al., 1998; Xie et al., 2011; Zhou et al., 2003, 2005, 2006; Zhou et al., 2008a, b; Cai et al., 2002; Kim and Cho, 2003; Hao et al., 2004; Wu et al., 2013, 2014; Wan et al., 2005, 2012; SD4IGMR, 2005; Wan et al., 2005, 2006, 2011, 2012; Li and Zhao, 2007; Tam et al., 2011, 2012a, b, c; Zhao and Zhai, 2013; Liu et al., 2013a, b; Zhao et al., 2010, 2011, 2012; Lu et al., 2004a, b, 2005, 2006; Lu et al., 2008; Wu et al., 2013, 2014; Meng et al., 2014; Liu et al., 2017a, 2017b, 2018a, 2018b, 2019a, 2019b; Zhou et al., 2001, 2003, 2005, 2006; Zhou et al., 2008a; Zhang et al., 2018; Oh et al., 2019; Xu et al., 2018b, 2018a, 2020; Xu and Liu, 2019; Lee et al., 2019). Models for explaining the origin of the JLJB include: 1) opening (at ~2.2 Ga) and closing (at ~1.9 Ga) of an intracontinental rift (Zhang and Yang, 1988; Li et al., 2004, 2005a, 2005b, 2006, 2012; Luo et al., 2004, 2008 Li and Zhao, 2007; Li et al., 2012), 2) arc-continent collision (Bai, 1993; Faure et al., 2004; Lu et al., 2006), and 3) a combination of the two previous scenarios with intracontinental rifting progressing to formation of a new ocean basin or back-arc basin, which was subsequently closed by subduction (Zhao et al., 2011; Zhao and Zhai, 2013; Zhang et al., 2018; Xu and Liu, 2019). Integrated studies considering geochronology, metamorphic and igneous petrology, geochemistry, structural geology and crustal structure are necessary to distinguish between these models.

Here we present new whole rock geochemical and isotopic data from the mafic/ultramafic metamorphic rocks (amphibolites, hornblendites, anthophyllite-rich rock and metagabbro) in the North Liaohe Group (and one sample from the South Liaohe Group) of the JLJB on the Liaodong Peninsula (Figs. 1B and 2). Whole rock analysis potentially allow access to portions of the geologic record that are not accessible through zircons alone, since they effectively sample a larger chemical equilibration volume and are potentially robust on the centimeter to meter scale despite high grade metamorphism and metasomatism. Further, integrated whole rock analysis of mafic rocks across a terrane potentially allows insights into mantle (lithospheric and asthenospheric) processes operating on the regional scale. Application of whole rock data in the context of existing zircon geochronology therefore offers a powerful tool for resolving the time-integrated thermal evolution of the terrane and construction of geodynamic models.

Hence, through integration of previously published results from the entire JLJB with our new whole rock geochronological and geochemical data from mafic/ultramafic meta-igneous rocks, we present a new model for the geodynamic evolution of the JLJB from ~2.8–1.7 Ga.

2. Regional geology

The JLJB is located in the northeastern part of the Eastern Block of the North China Craton (Fig. 1A). The northeast-southwest-trending belt is ~50–300 km wide and extends for ~1200 km from the eastern Jilin, via the eastern Liaoning, to the eastern Shandong province. Its central segment is situated between the Archaean Northern Liaoning-Northern Jilin Complex (Longgang Block) and the Archaean Southern Liaonan-Nangrim Complex (Nangrim Block). Its southern segment stretches across the Bohai Strait into the Archaean Eastern Shandong Complex on the Jiaodong Peninsula. The geology of the JLJB is summarized by Li et al., 1996, 2006, Li et al., 2011a, 2012; Li et al., 1997a; Li et al., 1997b, Li and Zhao (2007), Liu and Li (1996), Tam et al. (2011, 2012a, b, c) and Xu and Liu (2019). The JLJB consists of deformed and metamorphosed (up to high pressure granulite facies; Zhou et al., 2004, 2008a) volcanic and sedimentary sequences, granitoid and gabbroic intrusives, and mafic dikes (Fig. 1B). The volcanic and sedimentary sequences are

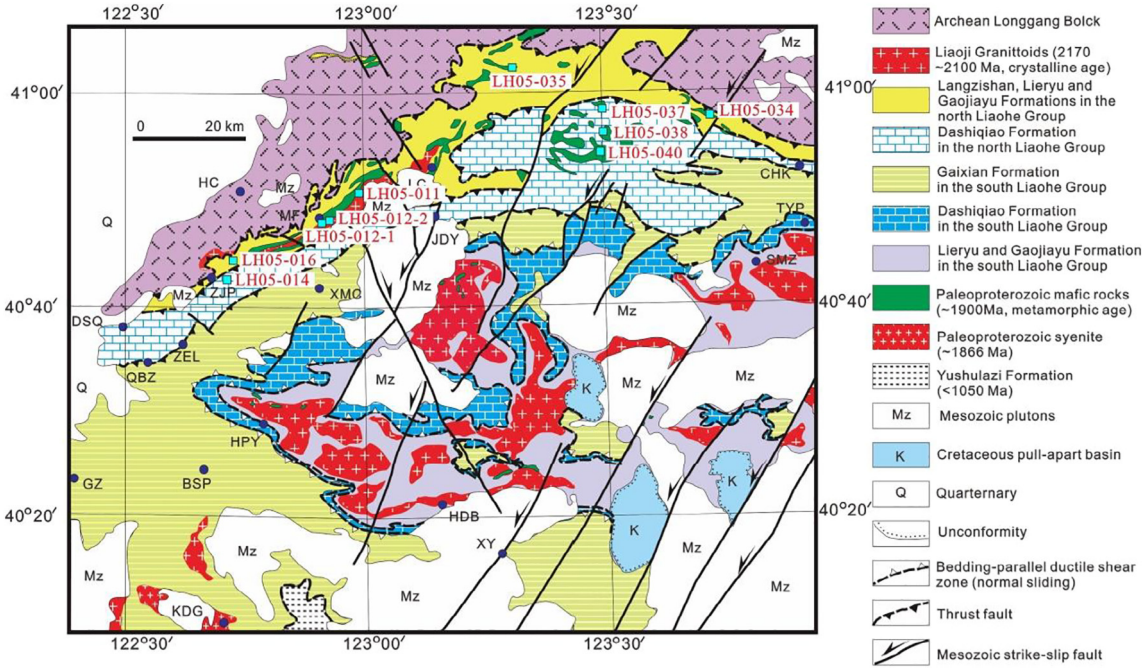

Fig. 2. Detailed map of the study area within the Jiao-Liao-Ji Belt showing sample locations. Mz-Mesozoic plutons, K-Cretaceous basins, Q-Quaternary. XY-Xiuyan County, HDB-Hadabei Town, KDG-Kuangdonggou Town, BSP-Bangshipu Town, HPY-Hupiyu Town, GZ-Gaizhou County, DSQ-Dashiqiao City, HC-Haicheng City, QBZ-Qingbaizhai Town, ZEL-Zaoerling Town, ZJP-Zhaojiapu Town, MF-Mafeng Town, LC-Longchang Town, JDY-Jidongyu Town, XMC-Ximucheng Town, CHK-Caohekou Town, TYP-Tongyuanpu Town, SMZ-Simenzi Town. The blue squares mark sample locations with sample labels shown in red next to the squares. (For interpretation of the references to colour in this figure legend, the reader is referred to the web version of this article.)

referred to (going from north to south) as the Laoling and Ji'an groups in southern Jilin (Lu et al., 2004a, b, 2005) and possibly the Macheonayeong Group in North Korea, the South and North Liaohe groups in eastern Liaoning, the Fenzishan and Jingshan groups, part of the Jiaobai Terrane in eastern Shandong on the Jiaodong Peninsula (Zhou et al., 2004, 2008a). The stratigrahic succession is transitional from a clastic-rich and bimodal volcanic sequence at the base through a middle carbonate-rich sequence to an upper pelitic sequence (Luo et al., 2004; Li et al., 2005a). The JLJB can be subdivided into a northern sub-belt, including the Laoling, North Liaohe and Fenzishan groups, and a southern sub-belt, including the Ji'an, South Liaohe and Jingshan groups. Faults and ductile shear zones separate these two sub-belts (Li et al., 2005a). The Liaohe Group, in the central portion of the belt, has been subdivided (going from bottom to top) into the Langzishan, Li'eryu, Gaojiayu, Dashiqiao and Gaixian formations, with the lowermost Langzishan Formation only being found in the North Liaohe Group (e.g., Li et al., 2005a; Dong et al., 2019). The Ji'an Group from bottom to top is subdivided into the Mayihe, Huangchagou and Dadongcha formations. The Laoling Group can be divided from bottom to top into the Dataishan (Linjiagou), Zhenzhumen, Huashan, Linjiang and Dasuzi formations. In the south, the Jingshan Group is divided from bottom to top into the Lugezhuang, Yetou and Douya formaitons, while the Fenzishan Group is divided from bottom to top into the Xiaosong, Zhujiakuang, Zhanggezhuang, Jutun and Gangyu formations (Liu et al., 2015).

The Eastern Block of the North China Craton has undergone a complex evolution since the Archean. Its earliest crustal formation events are recorded in the Anshan Complex, extending back to ~3.8 Ga (Liu et al., 1992; Song et al. 1996; Wan et al., 2012). Trondjemite-tonalite-granodiorite (TTG) gneisses provide evidence for a major phase of crustal growth at ~2.7 Ga, followed by alkaline granite emplacement along the northern margin of the JLJB at ~2.5 Ga. All of these units underwent dome-like deformation at ~2.5 Ga, which was distinct from the post-Archean deformation (Jahn et al., 2008; Zhao et al., 2005). The ~2.2–1.9 Ga NNE-trending Liaohe Group unconformably overlies the Neoarchean oval-shaped domes (Li et al., 2005a, 2005b, 2012; Luo et al., 2004, 2008).

3. Description of rock types

Ten mafic (amphibolites, hornblendites and a metagabbro) and one ultramafic (anthophyllite-rich rock) meta-igneous rocks from the Liaohe Group were selected for geochemical analyses in this study (see Table 1 and Figs. 1, 2). They form layers, blocks or lenses in the Liaohe Group, which have intrusive or tectonic contacts with the Liaoji Granitoids (Li et al., 2005a). All but one sample are from the North Liaohe Group (Fig. 2) and the remaining sample (LH05–26-1) from the South Liaohe Group (Fig. 1B).

The amphibolites, consisting of 50–60% hornblende and 40–50% plagioclase, have undergone low- to medium-grade metamorphism (lower-amphibolite facies; 0.3–0.8 Gpa; 500–700 °C; Li et al., 2001b) but extensive deformation (Li et al., 2005a). The metagrabbro sample consists of ~45% pyroxene, 10% hornblende converted from pyroxene, and ~45% plagioclase and shows evidence of lower-grade metamorphism (lower-greenschist facies; 0.3–0.5 Gpa; 350–450 °C; Li et al., 2001b). The hornblendites, consisting of ~90% hornblende and ~ 10% plagioclase, show signs of medium-grade metamorphism (lower-amphibolite facies; 0.4–1.0 Gpa; 500–650 °C; Li et al., 2001b). The anthophyllite-rich rock consists of 90% anthophyllite amphibole (lower-amphibolite facies; 0.3–0.8 Gpa; 550–650 °C; Li et al., 2001b). Protoliths of hornblendites and amphibolites were mafic (basaltic) volcanic rocks, whereas the anthophyllite-rich rock was most likely derived from an ultramafic protolith (possibly pyroxenite).

4. Analytical methods (major and trace element and isotope ratios)

Major and trace element data are shown in Table 1, Sr-Nd-Hf isotope data in Table 2, and Pb isotope data in Table 3. Major elements and selected trace elements (V, Zn, Ba, Sr and Zr) were determined on a Phillips X'Unique PW1480 X-ray fluorescence spectrometer

Table 1
Major and trace element geochemical data for the Liaohe mafic/ultramafic rocks. Abbreviations: anthophy. = anthophyllite, amph. = amphibolite, m-gab. = metagabbro, hbl. = hornblendite. [a] Replicate.

		LH05	LH05	LH05	LH05	LH05	LH05	LH05	LH05	LH05	LH05	LH05	LH05
Sample		011–1	012–1	012–2	014–7	016–1	026–1	034–1	034–1[a]	035-4	037-5	038-1	040–1
Rock Type		amph.	amph.	anthophy.	amph.	m-gab.	amph.	hbl.	hbl.	hbl.	hbl.	amph.	amph.
XRF													
SiO_2	%	50.69	54.86	40.51	57.58	49.71	49.47	45.49		49.39	49.22	49.26	49.59
TiO_2	%	0.95	0.51	0.23	0.68	1.22	1.25	2.96		2.14	1.52	1.38	1.02
Al_2O_3	%	13.88	9.51	4.25	17.18	13.26	13.49	12.72		13.2	12.72	14.22	12
Fe_2O_3	%	12.31	9.4	13.18	10.69	14.57	14.76	21.43		17.6	17.22	13.96	13.09
MnO	%	0.2	0.18	0.16	0.05	0.18	0.23	0.26		0.19	0.18	0.18	0.21
MgO	%	7.85	11.92	28.47	3.51	7.09	7.41	3.98		5.97	6.92	7.24	10.59
CaO	%	10.81	9.79	2.41	2.28	9.64	8.36	8.99		6.58	7.43	10.39	10.29
Na_2O	%	2.36	1.52	<0.01	1.45	2.53	2.46	2.24		1.73	2.09	1.55	2.4
K_2O	%	0.55	1.01	0.01	5.36	0.78	1.51	1.18		2.14	0.75	0.95	0.12
P_2O_5	%	0.07	0.07	0.04	0.07	0.12	0.12	0.15		0.23	0.15	0.15	0.07
V	ppm	265	391	95	105	309	289	751		376	347	250	262
Zn	ppm	83	69	96	87	64	116	143		97	78	108	91
Ba	ppm	118	226	42	624	129	438	365		610	130	139	<8
Sr	ppm	199	126	25	449	158	314	180		114	130	204	94
Zr	ppm	52	64	28	135	86	79	113		167	133	116	67
H_2O	%	1.53	1.93	9.34	1.89	1.97	2.17	1.47		1.58	3.04	1.77	1.45
CO_2	%	0.03	0.04	0.75	0.07	0.05	0.13	0.47		0.2	0.33	0.21	0.04
TOTAL		101.33	100.92	99.60	101.07	101.24	101.55	101.54		101.14	101.70	101.44	101.00
ICPMS_Parr© Bomb Digest													
Li	ppm	37.5	22.3	0.882	37.9	14.5	21.6	11.8	11.8	21.0	26.1	9.79	3.83
Sc	ppm	44.0	46.1	14.1	31.3	46.3	42.9	41.3	37.8	38.5	42.0	32.8	41.9
V	ppm	261	385	86.5	106	321	290	774	724	373	339	244	249
Cr	ppm	53.5	1019	864	140	167	98.5	16.3	15.1	79.4	41.7	332	377
Co	ppm	40.7	44.7	122	42.7	47.8	53.3	60.5	58.1	47.0	53.2	49.1	47.1
Ni	ppm	37.0	64.4	1253	75.6	67.5	48.9	19.8	18.9	40.3	35.7	103	70.1
Cu	ppm	24.9	18.3	205	11.5	31.4	31.0	36.5	37.0	18.1	31.5	50.8	5.01
Zn	ppm	75.9	70.1	96.5	89.5	67.2	113	141	140	99.0	79.6	103	87.5
Ga	ppm	15.9	11.8	5.57	21.8	17.3	16.6	24.0	23.5	21.0	18.7	18.8	10.4
Rb	ppm	31.1	60.6	0.512	166	22.7	89.0	36.0	35.5	102	25.6	33.0	1.12
Sr	ppm	191	121	23.2	410	155	303	177	174	108	122	193	90.3
Y	ppm	15.8	15.7	5.55	13.8	27.0	25.5	30.1	29.9	41.0	30.5	26.9	18.0
Zr	ppm	46.8	70.6	29.3	146	87.8	77.1	104	102	155	126	115	65.1
Nb	ppm	2.75	3.59	1.78	8.16	4.75	4.47	7.30	7.14	8.88	6.68	6.86	3.36
Mo	ppm	0.428	0.108	0.301	0.055	0.253	0.154	0.469	0.485	0.528	0.435	0.549	0.128
Cs	ppm	0.289	1.75	0.727	7.85	0.247	1.05	0.756	0.748	16.4	0.731	0.733	0.039
Ba	ppm	119	244	6.12	634	162	443	372	370	595	118	195	19.4
La	ppm	4.56	10.9	3.33	30.2	6.74	7.40	9.50	9.46	13.1	9.58	13.7	3.40
Ce	ppm	10.7	22.9	7.37	57.3	16.6	17.0	22.8	22.6	31.3	23.4	30.3	11.0
Pr	ppm	1.57	2.81	0.937	7.37	2.53	2.43	3.246	3.24	4.51	3.37	3.99	1.64
Nd	ppm	7.46	11.3	3.84	28.2	12.1	11.3	15.3	15.3	21.0	16.2	17.3	8.22
Sm	ppm	2.14	2.54	0.901	5.21	3.54	3.12	4.27	4.23	5.69	4.56	4.32	2.46
Eu	ppm	0.858	0.570	0.164	1.14	1.25	1.08	1.60	1.60	1.95	1.49	1.40	0.681
Gd	ppm	2.54	2.60	0.930	4.32	4.23	3.83	5.01	4.96	6.66	5.28	4.73	2.92
Tb	ppm	0.439	0.427	0.156	0.588	0.733	0.671	0.855	0.848	1.14	0.905	0.783	0.507
Dy	ppm	2.86	2.75	1.00	3.09	4.80	4.46	5.52	5.50	7.43	5.81	4.98	3.31
Ho	ppm	0.592	0.566	0.205	0.543	0.984	0.932	1.13	1.12	1.52	1.18	1.00	0.679
Er	ppm	1.63	1.60	0.590	1.39	2.73	2.62	3.12	3.07	4.21	3.25	2.73	1.86
Tm	ppm	0.241	0.240	0.090	0.195	0.400	0.389	0.454	0.450	0.609	0.482	0.398	0.270
Yb	ppm	1.57	1.59	0.606	1.32	2.61	2.59	2.98	2.97	3.86	3.15	2.58	1.74
Lu	ppm	0.242	0.243	0.095	0.220	0.393	0.398	0.457	0.452	0.558	0.476	0.391	0.263
Hf	ppm	1.26	1.78	0.729	3.65	2.23	1.97	2.80	2.76	4.03	3.33	2.97	1.69
Ta	ppm	0.168	0.233	0.108	0.524	0.274	0.272	0.429	0.425	0.527	0.402	0.424	0.222
Tl	ppm	0.157	0.298	0.101	0.454	0.108	0.555	0.167	0.164	1.59	0.128	0.226	0.012
Pb	ppm	1.97	3.37	1.66	7.44	0.804	8.07	2.53	2.54	12.4	1.98	2.28	1.61
Th	ppm	0.712	3.08	1.04	7.73	0.998	1.07	1.60	1.53	2.00	1.69	3.19	1.28
U	ppm	0.216	0.820	0.254	1.14	0.321	0.270	0.416	0.397	0.563	0.471	0.886	0.202

[a] Replicate.

(XRF) at GEOMAR using fused beads. H_2O and CO_2 were determined by infrared photometry on a Rosemount CSA 5003. Values determined on reference samples JB-2, JB-3, JA-2 and JR-1, measured along with the samples, lie within 5% of Jochum et al. (2016) for JB-2 and JA-2 and Govindaraju (1994) for JB-3 and JR-1 for the major elements, except MnO in JB-2, and at several tenth weight percent of TiO_2, MgO and CaO in JR-1. V, Zn, Ba, Sr and Zr generally deviate by <10% from reference values except V in JA-2. For details on XRF standard materials see Appendix A2.

Solution ICPMS analyses for trace elements were carried out on an Agilent 7500cs instrument at the Institute of Geosciences at Kiel University following the methods of Garbe-Schönberg (1993). Initial sample digestion was done in Parr© pressure digestion vessels in an oven at 120 °C for 4 days. Reference material BHVO-2, BIR-1 and JGb-2 (two dissolutions) were prepared and measured along with the samples. See Appendix 3a for ICP-MS standard analyses. JGb-2 replicates within 1.7 ± 1.5% (1SD) except Zn (7.8%), Zr (21.9%) and Mo (35.2%). Sample 34–1 was replicated at 2.1 ± 1.6% (1SD) except Sc (12.7%), V (9.4%)

Table 2
Sr-Nd-Hf isotope data for the Liaohe mafic/ultramafic rocks. Abbreviations: anthophy. = anthophyllite, amph. = amphibolite, m-gab. = metagabbro, hbl. = hornblendite.

Field Campaign	LH05	LH05	LH05	LH05	LH05	LH05	LH05	LH05	LH05	LH05	LH05	LH05
Sample	011–1	012–1	012–2	014–7	016–1	026–1	034–1[b]	035–4	037–5	038–1	040–1	040–1[a]
Rock Type	amph.	amph.	anthophy.	amph	m-gab.	amph.	hbl.	hbl.	hbl.	amph.	amph.	amph.
$^{87}Sr/^{86}Sr$	0.713939	0.737525	0.742426	0.732517	0.716498	0.723869	0.719027	0.771028	0.716097	0.716973	0.704912	0.704909
2SE	0.000005	0.000006	0.000004	0.000006	0.000005	0.000006	0.000005	0.000005	0.000005	0.000006	0.000006	0.000005
$^{87}Rb/^{86}Sr_{ICP}$	0.472	1.455	0.064	1.170	0.426	0.850	0.590	2.761	0.609	0.494	0.036	0.036
$^{87}Sr/^{86}Sr_{\ t\ =1.671Ga}$	0.70260	0.70259	0.74089	0.70443	0.70628	0.70345	0.70485	0.70473	0.70148	0.70510	0.70405	0.70405
$^{143}Nd/^{144}Nd$	0.512350	0.511686	0.511676	0.511341	0.512471	0.512268	0.512268	0.512336	0.512419	0.511912	0.512419	0.512414
2SE	0.000005	0.000005	0.000006	0.000005	0.000005	0.000005	0.000005	0.000005	0.000005	0.000005	0.000006	0.000003
εNd	−5.62	−18.57	−18.77	−25.29	−3.25	−7.21	−7.22	−5.90	−4.27	−14.16	−4.27	−4.37
$^{147}Sm/^{144}Nd_{ICP}$	0.173	0.135	0.141	0.111	0.176	0.167	0.167	0.163	0.169	0.151	0.180	0.180
$^{143}Nd/^{144}Nd_{\ t\ =2.83Ga}$	0.50912	0.50917	0.50903	0.50927	0.50919	0.50915	0.50915	0.50929	0.50926	0.50910	0.50905	0.50904
$\varepsilon Nd_{\ t\ =2.83Ga}$	3.03	3.95	1.36	5.89	4.45	3.68	3.57	6.38	5.82	2.66	1.62	1.52
$^{176}Hf/^{177}Hf$	0.282618	0.282190	0.282159	0.281774	0.282578	0.282656	0.282455	0.282385	0.282446	0.282207	0.282405	0.282405
2SE	0.000008	0.000010	0.000016	0.000004	0.000007	0.000007	0.000006	0.000007	0.000005	0.000014	0.000009	0.000009
εHf	−5.44	−20.59	−21.67	−35.28	−6.87	−4.12	−11.21	−13.69	−11.53	−19.99	−12.98	−12.98
$^{176}Lu/^{177}Hf_{ICP}$	0.028	0.020	0.019	0.009	0.025	0.029	0.023	0.020	0.020	0.019	0.022	0.022
$^{176}Hf/^{177}Hf_{\ t\ =2.25Ga}$	0.28140	0.28132	0.28133	0.28139	0.28146	0.28137	0.28142	0.28150	0.28154	0.28137	0.28141	0.28141
$\varepsilon Hf_{\ t\ =2.25Ga}$	3.46	0.84	1.23	3.27	5.63	2.52	4.20	7.31	8.47	2.58	4.11	4.11

[a] Replicate.
[b] P/D uses average of replicate analysis.

and Cr (11.1%). See Appendix 3b for details of sample replicates. The accuracy of BIR-1 lies within 4.0 ± 2.6% (1SD) of the preferred GeoReM values of Jochum et al. (2016) except Tl (67.1%) and U (29.1%). For BHVO-2 deviations of 1.5 ± 1.1% (1SD) from GeoReM values are observed except Sr (6.0%), Mo (10.1%), Hf (6.9%), Ta (9.2%) and Th (5.9%). For the less well characterized JGb-2 material, deviations of 8.7 ± 5.6% (1SD) are observed from compiled GeoReM values (http://georem.mpch-mainz.gwdg.de/). Larger deviations exist for Nb (47.6%), Mo (28.3%), Cs (20.2%), Ta (94.7%), Tl (38.9%) and Pb (48.2%).

Sr-Nd-Pb isotope analyses were undertaken at GEOMAR on TRITON (Sr—Nd) and MAT262 (Pb) thermal ionization mass spectrometers. Circa 100 mg of unleached sample powders were used for the isotope analyses. Chemical separation of Sr, Nd and Pb followed the chromatographic principles outlined in Jacques et al. (2013) and references therein. Isotope ratios were determined in static multi-collection mode with Sr and Nd being mass bias corrected to $^{86}Sr/^{88}Sr = 0.1194$ and $^{146}Nd/^{144}Nd = 0.7219$ for each integration, while Pb was externally corrected by applying 0.113‰ / amu to the measured Pb isotope ratios. The fractionation factor is based on repeat measurements of NBS981 and normalization to the values of Todt et al. (1996). The external 2SD errors of NBS981 (n = 195) are ~200 ppm / amu and translate to 2SD errors of 0.0445%, 0.0607% and 0.0797% for $^{206}Pb/^{204}Pb$, $^{207}Pb/^{204}Pb$ and $^{208}Pb/^{204}Pb$ respectively. $^{87}Sr/^{86}Sr$ and $^{143}Nd/^{144}Nd$ sample ratios are reported relative to $^{87}Sr/^{86}Sr = 0.710250 \pm 0.000006$ (n = 5; 2SD) for NBS987 and $^{143}Nd/^{144}Nd = 0.511850 \pm 0.000006$ (n = 10; 2SD) for La Jolla. Hf chemistry followed the methods of Blichert-Toft et al., 1997, and $^{176}Hf/^{177}Hf$ was determined on a Nu-Plasma MC-ICPMS at GEOMAR. The long-term (2011–2018) standard bracketing normalized value of the in-house Hf SPEX CertiPrep ™ solution is $^{176}Hf/^{177}Hf = 0.282170 \pm 0.000006$ (2SD, n = 553) corresponding to $^{176}Hf/^{177}Hf = 0.282163$ for JMC475. Sr-Nd-Hf-Pb replicate analysis of LH05-040-1 lie within 2SD of the standards (Tables 2 and 3). Age calculations were conducted using a root sum of squares approach to propagate the external 2SD of the isotope standards and a conservative 5% 2 sigma error from parent/daughter ratios. For regressions that returned MSWD values which were less than the appropriate value for the number of samples in the regression (typically MSWD = 1.89 for n = 10) no further error magnification was applied. For those above the target

Table 3
U-Th-Pb isotopic data for the Liaohe mafic/ultramafic rocks. Abbreviations: anthophy. = anthophyllite, amph. = amphibolite, m-gab. = metagabbro, hbl. = hornblendite.

Field Campaign	LH05	LH05	LH05	LH05	LH05	LH05	LH05	LH05	LH05	LH05	LH05	LH05
Sample	011–1	012–1	012–2	014–7	016–1	026–1	034–1[b]	035–4	037–5	038–1	040–1	040–1[a]
Rock Type	amph.	amph.	anthophy.	amph.	m-gab.	amph.	hbl.	hbl.	hbl.	amph.	amph.	amph.
$^{206}Pb/^{204}Pb$	21.679	20.797	19.128	19.960	23.134	19.762	19.169	17.006	23.849	28.006	18.989	18.968
2SE	0.003	0.001	0.001	0.001	0.001	0.001	0.001	0.001	0.001	0.001	0.001	0.001
$^{207}Pb/^{204}Pb$	16.024	15.840	15.691	15.787	16.118	15.847	15.777	15.551	16.337	16.763	15.663	15.658
2SE	0.002	0.001	0.001	0.000	0.001	0.000	0.001	0.001	0.001	0.001	0.001	0.001
$^{208}Pb/^{204}Pb$	40.389	40.930	38.548	43.084	45.147	39.072	39.780	36.620	42.623	47.806	40.669	40.636
2SE	0.005	0.001	0.002	0.001	0.003	0.001	0.003	0.002	0.003	0.002	0.002	0.001
$^{207}Pb/^{206}Pb$	0.73918	0.76163	0.82032	0.79092	0.69671	0.80188	0.82306	0.91444	0.68500	0.59855	0.82483	0.82545
2SE	0.00001	0.00001	0.00001	0.00001	0.00001	0.00001	0.00001	0.00001	0.00001	0.00001	0.00001	0.00001
$^{208}Pb/^{206}Pb$	1.86303	1.96802	2.01520	2.15846	1.95144	1.97711	2.07515	2.15333	1.78712	1.70692	2.14165	2.14225
2SE	0.00003	0.00003	0.00005	0.00003	0.00002	0.00003	0.00002	0.00003	0.00005	0.00002	0.00004	0.00002
$^{238}U/^{204}Pb_{ICP}$	7.49	16.52	9.83	10.54	29.45	2.19	10.50	2.76	17.24	31.43	8.26	8.25
$^{235}U/^{204}Pb_{ICP}$	0.054	0.120	0.071	0.076	0.214	0.016	0.076	0.020	0.125	0.228	0.060	0.060
$^{232}Th/^{204}Pb_{ICP}$	25.51	64.09	41.48	74.11	94.68	8.93	41.80	10.14	63.82	116.99	54.13	54.09
$^{232}Th/^{238}U_{ICP}$	3.41	3.88	4.22	7.03	3.22	4.08	3.98	3.68	3.70	3.72	6.56	6.56
$^{206}Pb/^{204}Pb_{\ t\ =1.824Ga}$	19.23	15.40	15.91	16.51	13.50	19.05	15.73	16.10	18.21	17.73	16.29	16.27
$^{207}Pb/^{204}Pb_{\ t\ =1.824Ga}$	15.75	15.24	15.33	15.40	15.04	15.77	15.39	15.45	15.71	15.62	15.36	15.36
$^{208}Pb/^{204}Pb_{\ t\ =1.824Ga}$	37.98	34.88	34.63	36.09	36.21	38.23	35.83	35.66	36.60	36.76	35.56	35.53
$^{207}Pb/^{206}Pb_{\ t\ =1.824Ga}$	0.82	0.99	0.96	0.93	1.11	0.83	0.98	0.96	0.86	0.88	0.94	0.94
$^{208}Pb/^{206}Pb_{\ t\ =1.824Ga}$	1.98	2.27	2.18	2.19	2.68	2.01	2.28	2.21	2.01	2.07	2.18	2.18

[a] Replicate.
[b] P/D uses average of replicate analysis.

MSWD, the error has been multiplied by the square root of the MSWD, highlighting additional sources of error beyond analytical uncertainty. See Table 4 for further discussion regarding the MSWD.

5. Results

5.1. Major and trace element compositions for the Liaohe mafic meta-igneous rocks

The amphibolites, excluding sample LH05–14-7, generally have higher SiO_2 (49.3–54.9 wt%), MgO (7.2–11.9 wt%) and CaO (7.2–10.8 wt%) but lower FeO^t (8.5–13.3 wt%) and TiO_2 (0.5–1.4 wt%) than the higher-grade metamorphic hornblendites (SiO_2 = 45.5–49.4 wt%; MgO = 4.0–6.9 wt%; CaO = 6.6–9.0 wt%; FeO^t = 15.5–19.3 wt%; TiO_2 = 1.5–3.0 wt%). The composition of the metagabbro is similar to that of the amphibolites (SiO_2 = 49.7 wt%; MgO = 7.1 wt%; FeO^t = 13.1 wt%; CaO = 9.6 wt%; TiO_2 = 1.2 wt%). No systematic differences exist between the aforementioned rock types in Al_2O_3 (9.5–14.2 wt%), Na_2O (1.5–2.5 wt%) and K_2O (0.1–2.1 wt%). All of the samples have basaltic whole rock compositions. Amphibolite sample LH05–14-7 has a distinct composition from the other amphibolites, metagabbro and hornblendites, displaying the highest SiO_2 (57.6 wt%), Al_2O_3 (17.2 wt%) and K_2O (5.4 wt%), lowest MgO (3.5 wt%) and CaO (2.3 wt%), and second lowest FeO^t (9.6 wt%) and TiO_2 (0.7 wt%). It has an andesitic type chemical composition. Compared to all other samples, the anthophyllite-rich rock has the lowest SiO_2 (40.5 wt%), Al_2O_3 (4.2 wt%), TiO_2 (0.2 wt%) and nearly the lowest CaO (2.4 wt%) but highest MgO (28.5 wt%) and intermediate FeO^t (13.2 wt%).

The Liaohe mafic rocks generally show relative enrichments in fluid-mobile elements, such as Cs, Rb, Ba, U, K and Pb (Fig. 3). The only exception is the anthophyllite-rich rock, which has relative depletions in Rb, Ba, K and Sr. These elements are likely to have been removed during metamorphism. All samples show distinct relative depletion in Nb and have relatively flat heavy rare earth element (HREE) patterns with the exception of amphibolite LH05–014–7, which also has distinct major element composition compared to all other samples. LH05–014–7 has the highest incompatible element abundances and the highest immobile more to less incompatible element ratios, such as La/Yb, Nb/Yb and Th/Yb.

Table 4
Summary of whole rock isochron data for the Liaohe mafic/ultramafic units. All regressions based on bomb dissolution including at least one duplicate (n = 11) with the exception of Sr (n = 10). Tremolite LH-05-012-2 not included in regressions. Isochron plots in Figs. 4–6. Abbreviations: conv = conventional; inv. = inverse.

System	Age	±2 SE	initial	±2SE	MSWD	±2SE no MSWD*
	Ga	*Ga*				*Ga*
^{147}Sm-^{143}Nd	2.833	0.180	0.50935	0.00039	1.2	0.180
^{176}Lu-^{176}Hf	2.251	0.310	0.28141	0.00029	1.3	0.310
^{207}Pb-^{206}Pb conv	1.865	0.599			44.3	0.090
^{207}Pb-^{206}Pb inv	1.824	0.019	0.1115	0.0068	1	0.019
^{232}Th-^{208}Pb	1.699	3.711	36.7	1.2	128	0.178
^{87}Rb–^{87}Sr	1.671	0.058	0.70404	0.00120	2.3	0.039
^{235}U-^{207}Pb	1.636	2.911	15.6	0.2	265	0.179
^{238}U-^{206}Pb	1.534	5.044	17.4	1.7	370	0.262

* for regressions of 11 samples, the target MSWD = 1.89, as based upon the ratio of the minimization parameter (S) and the degrees of freedom in the system (2). Standard practice has been to multiply the error of the regression by the square root of the MSWD when the regressions return a MSWD>target, hence reflecting the greater uncertainty within the regression than implied by the assigned analytical uncertainties. We include here for reference the associated errors which have not had the a priori MSWD multiplication, since there may be non-geological sources of error and hence the non-corrected errors allow some sense of "errorchron" age ranges beyond the conventional statistical evaluation.

5.2. Sm—Nd, Lu—Hf, U-Th-Pb and Rb—Sr age data for the Liaohe mafic meta-igneous rocks

Whole rock regressions have been conducted for ^{147}Sm—^{144}Nd (Fig. 4A), ^{176}Lu—^{177}Hf (Fig. 4B), ^{87}Rb—^{86}Sr (Fig. 5), ^{207}Pb—^{206}Pb (Fig. 6), ^{238}U—^{206}Pb (Appendix 4A), ^{235}U—^{207}Pb (Appendix 4B), and ^{232}Th—^{208}Pb (Appendix 4C), excluding the sample LH05 012–2 (anthophyllite-rich rock). The results are summarized in Table 4.

In summary, ^{147}Sm—^{144}Nd preserves a whole rock isochron age (Fig. 4A), which predates the age of the surrounding sedimentary package in which the mafic igneous rocks are hosted. The 10 mafic meta-igneous Liaohe samples yield a bulk-rock Sm—Nd isochron age of 2.83 ± 0.18 Ga, an initial $^{143}Nd/^{144}Nd$ ratio of 0.50935 ± 0.00039 (MSWD of 1.2). $\varepsilon Nd_{(2.83\ Ga)}$ ranges from +1.52 to +5.89 with one sample having a value of +6.38.

The ^{176}Lu—^{177}Hf bulk rock isochron of 2.25 ± 0.31 Ga (Fig. 4) lies just outside of the 2 sigma error of the Sm—Nd age but covers the age range of the related granites (2.2–2.0 Ga) based on zircon age dating (e.g. Zhou et al., 2008a, b). The initial $^{176}Hf/^{177}Hf$ = 0.28141 ± 00029 and $\varepsilon Hf_{(2.25Ga)}$ range from +0.85 − +8.48 with the majority around ~ + 3.5–4.5.

The ^{87}Rb—^{86}Sr system preserves a near isochronous relationship (MSWD = 2.3) at 1671 ± 58 Ma with an initial ratio of 0.70404 (Fig. 5). This initial ratio is relatively radiogenic and is consistent with derivation from a metamorphic or reset isochron.

An inverse ^{207}Pb—^{206}Pb isochron diagram yields a precise age of 1824 ± 19 Ma (MSWD =1; Fig. 6), whereas a conventional Pb—Pb isochron yields a far less precise, but overlapping age of 1.87 ± 0.60 Ga (MSWD = 44). Given the radiogenic nature of the measured ancient Pb isotopes and the correspondingly highly correlated errors and relatively low ^{204}Pb abundances, the inverse isochron approach is generally the favored for samples of this antiquity, and in the following discussion we consider this isochron as the preferred Pb—Pb isotope age in this sample suite.

Not surprisingly, U-Th-Pb isochron diagrams display varying degrees of open system behavior. Both U and Th are geochemically very different to Pb, and hence metamorphism and metasomatism will readily fractionate the parent element from the daughter. Nevertheless, all systems preserve broadly linear arrays with slopes corresponding to ~1.70, 1.64 and 1.53 Ga for $^{232}Th/^{204}Pb$ versus $^{208}Pb/^{204}Pb$, $^{235}U/^{204}Pb$ versus $^{207}Pb/^{204}Pb$ and $^{238}U/^{204}Pb$ versus $^{206}Pb/^{204}Pb$ respectively. The very high MSWD's for these regressions render propagation of errors on the ages of these regressions as geologically meaningless, however the simple errors generated by the spread of the data in the arrays (of the order of ~0.20 Ga) allow for these ages to reflect either cooling of the terrane or a subsequent, very young event, which only partially reset the U-Th-Pb system.

6. Discussion

6.1. Constraints on the age of formation and metamorphism of the Liaohe mafic meta-igneous rocks

The Liaohe mafic meta-igneous rocks form good positive linear correlations on the Sm—Nd, Lu—Hf, Rb—Sr and inverse $^{207}Pb/^{206}Pb$ isochron diagrams. Linear correlations on these isotope diagrams can either represent: 1) isochrons (or pseudo-isochrons) formed through radioactive decay of parent to daughter isotopes over extended time periods, or 2) two-component mixing in young samples or age-corrected older samples. Positive linear correlations of the measured isotopic composition on all isotope correlation diagrams in these presumed Paleoproterozoic rocks point to radiogenic ingrowth having formed these arrays, in particular since the linear arrays on all isotope correlation diagrams have positive slopes. Two-component mixing could also generate linear negative correlations. In addition, the Pb isotope ratios are more extreme than any

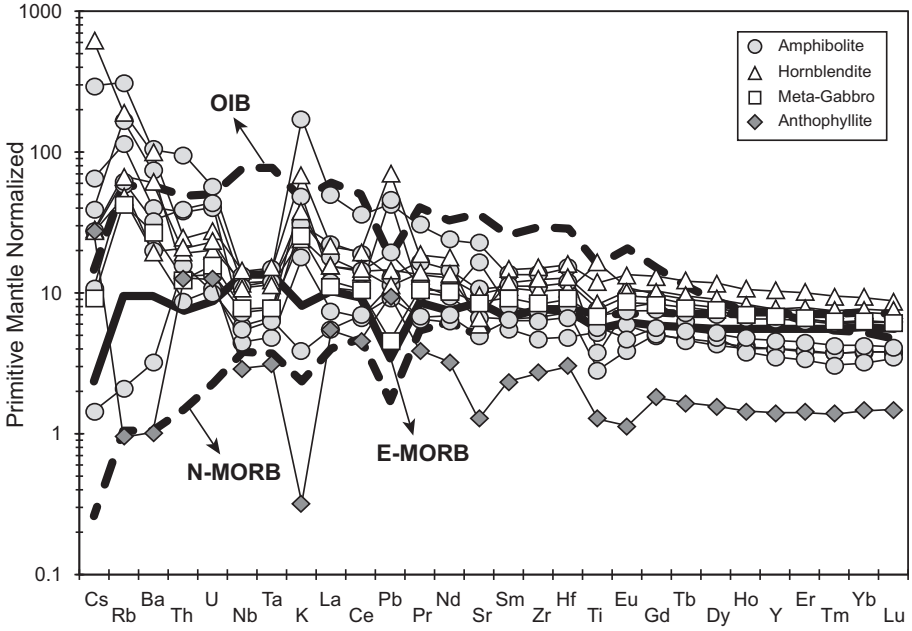

Fig. 3. Incompatible multi-element diagram showing the ten mafic meta-igneous (amphibolites, hornblendites and meta-gabbro) and one meta-ultramafic (anthophyllite-rich) rocks. Note the distinct negative Nb—Ta anomalies (troughs) and positive anomalies (peaks) for most fluid-mobile elements, such as Rb, Ba, K and Pb, in the incompatible-element patterns for the Liaohe rocks, in contrast to the positive anomalies (peaks) for Nb—Ta and lower concentrations of fluid-mobile elements in the incompatible-element patterns for normal mid-ocean-ridge basalt (N-MORB), enriched mid-ocean-ridge basalt (*E*-MORB) and ocean island basalt (OIB) patterns. These geochemical features point to generation of the Liaohe mafic melts in a subduction-zone setting rather than at an ocean spreading center (MOR) or in an intraplate tectonic setting. Abundances are normalized to primitive mantle after Hofmann, 1988. Reference patterns for ocean island basalt (OIB), normal mid ocean ridge basalt (N-MORB) and enriched (E-) MORB after Sun & McDonough, 1989.

Phanerozoic rocks that we are aware of and thus are likely to reflect radiogenic ingrowth of U and Th rather than two-component mixing. As discussed below, zircons dated from other rocks in the Jiao-Liao-Ji

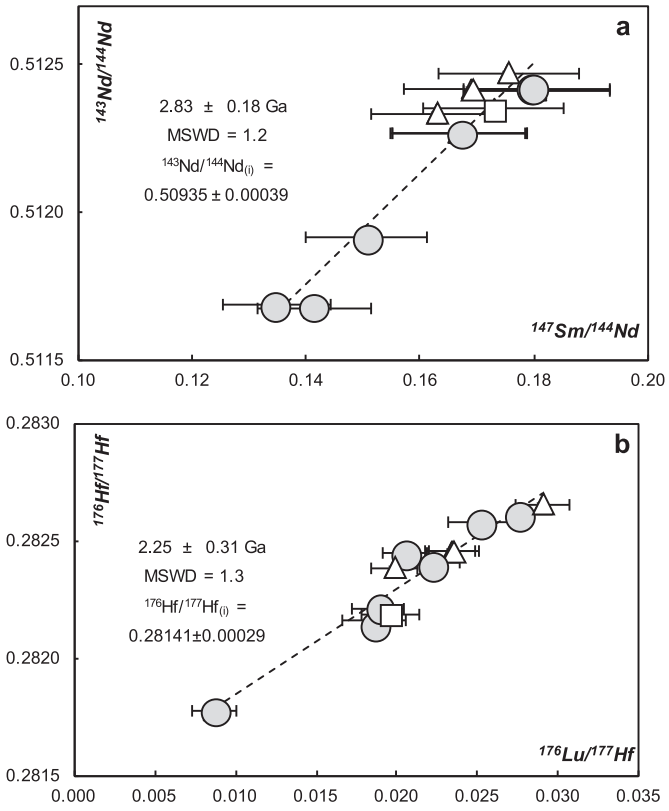

Fig. 4. a) Whole-rock Sm—Nd and b) whole-rock Lu—Hf isochrons for the Liaohe meta-mafic rocks. For symbols see Fig. 3.

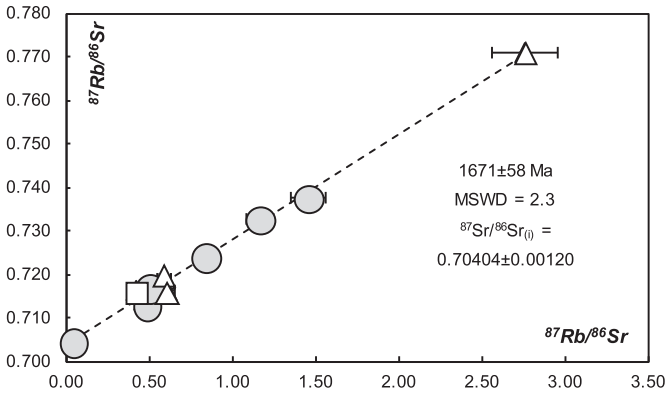

Fig. 5. Whole-rock Rb—Sr isochron diagram for the Liaohe meta-mafic rocks. For symbols see Fig. 3.

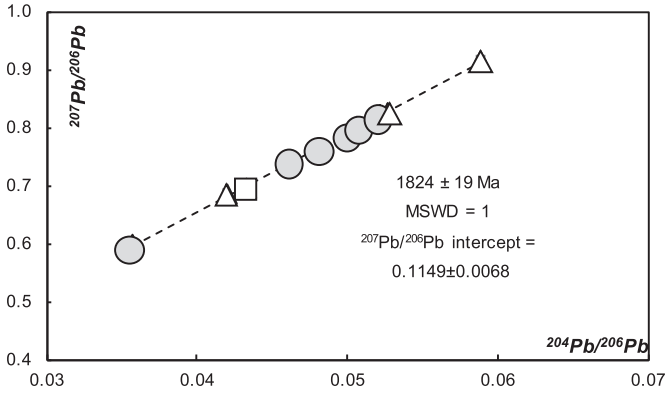

Fig. 6. Inverse whole-rock Pb—Pb isochron diagram for the Liaohe meta-mafic igneous rocks. For symbols see Fig. 3.

Belt have similar ages to those we report here for whole rocks. Alteration can affect parent-daughter ratios after emplacement, especially of Rb, Sr, U and Pb; however, Sm, Nd, Lu and Hf are generally fairly resistant to alteration and to metamorphism, through at least amphibolite metamorphic grade. Therefore, we interpret these linear arrays to form isochrons that provide age information about the origin and metamorphic history of the Liaohe mafic meta-igneous rocks.

Nine of the ten samples plotting on the Sm—Nd, Rb—Sr and $^{207}Pb/^{206}Pb$ isochrons come from the North Liaohe Group and therefore the age information strictly only applies to the North Liaohe Group. One sample from the South Liaohe Group, however, plots on all of the positive linear arrays formed by the North Liaohe samples, suggesting that the South Liaohe Group rocks, or at least some of them, were formed at a similar time and experienced a similar history to the North Liaohe Group rocks. Hence the bulk rock approach employed here explores processes that took place on lithospheric scales.

6.1.1. Sm—Nd and Lu—Hf isochrons: formation age of the mafic meta-igneous Liaohe rocks and their mantle source

Of the studied isotope systems, the Sm—Nd system is considered the most robust, due to the relative immobility of Sm and Nd (e.g., Schaefer, 2016). The excellent correlation of Zr with Sm ($r^2 = 0.98$) and Nd ($r^2 = 94$) and between Sm and Nd ($r^2 = 0.96$), excluding anomalous sample LH05-14-7, suggests that late-stage processes have not mobilized these elements. If post-emplacement mobilization due to alteration had taken place, it is unlikely that such a good correlation would have been preserved on the Sm—Nd isochron diagram. Therefore, we interpret the 2.83 ± 0.18 Ga Sm—Nd isochron age to reflect the age when Sm and Nd were last significantly fractionated from one another.

There are two possible interpretations for the Sm—Nd isochron: 1) The age is that of eruption/emplacement of the subsequently metamorphosed mafic rocks, or 2) the age reflects the stabilization/isolation of the mantle source from which these rocks were subsequently derived. On a whole rock scale, the latter scenario is plausible for large degrees of partial melting from sources that themselves contain uniform $^{143}Nd/^{144}Nd$ and Sm/Nd ratios. In the case of Precambrian rocks, these include previously depleted reservoirs, which have maintained closed-system behavior from the rest of the convecting mantle for extended periods of time. Examples of whole rock Sm—Nd isochrons preserving ages that are hundreds of million years older than their emplacement have been reported in the literature for quite some time - significantly these include Archaean komatiites (Chauvel et al., 1985), Proterozoic mafic dikes (Schaefer, 1998) and metamorphosed mafic and felsic intrusive rocks (e.g., Theriault and Ross, 1991; Zhao and McCulloch, 1995). Indeed, such occurrences are possibly relatively common; however, they are overlooked in preference to calculated model ages from the data, or the isochrons are simply ignored as other geological constraints clearly rule out older isochron ages representing the time of emplacement.

In the Liaohe mafic meta-igneous rocks, field relationships show some intrusive contacts with the Liaoji Granitoids (dated between 2.2 and 2.0 Ga with a peak at ~2.15 Ga; Zhou et al., 2008a, b; Meng et al., 2014; Wang et al., 2017; Zhang et al., 2018; Liu et al., 2019b) for some of the mafic outcrops, although others may be simply tectonically interleaved (Li et al., 2005a, 2005b). In any case, it is unlikely that the mafic protoliths were emplaced at ~2.83 Ga, therefore a younger emplacement age of ~2.2–2.1 Ga, similar to the major age range of the Liaoji Granitoids (e.g. Zhou et al., 2008a, b), seems to be the best age estimate for these rocks based on stratigraphic considerations. U—Pb dating of magmatic zircons from mafic meta-igneous rocks from the central Liaodong Peninsula (North Liaohe Group), similar to those studied here, yield two age groups: 1) 2547–2493 Ma, peak at 2503 Ma and 2) 2246–2135 Ma, peak at 2154 Ma with peak in T_{Hf} model ages at 2.19 Ga (Meng et al., 2014). The older ages are interpreted to be inherited zircons derived from melting of underlying 2.5 Ga crust, providing direct evidence for Archean crust beneath this part of the JLJB. Therefore, it is likely that the Sm—Nd isochron reflects the time of formation of the mantle source from which these rocks were derived. Below we summarize literature studies providing evidence that parts of the crust beneath the JLJB separated from the mantle as much as 3.9 Ga ago with major crustal growth stages at 3.0–2.9 Ga, 2.8–2.7 Ga and ~ 2.5 Ga, consistent with the 2.83 ± 0.18 Ga Sm—Nd whole rock isochron age reflecting lithospheric mantle stabilization between ~3.0–2.6 Ga. The younger zircon age group is interpreted to reflect the emplacement age of the meta-igneous protoliths, derived by partial melting of depleted lithospheric mantle metasomatized by subduction-zone fluids/melts. Lu—Hf age of 2.25 Ga is within error of the peak of the younger zircon group (2.15 Ga). Thus, it is reasonable to suggest that whole-rock Lu—Hf age records the emplacement of the mafic protoliths into the crust and that the emplacement of the Liaohe mafic rocks appears to have been contemporaneous with the more voluminous felsic magmatism and most likely reflects the mafic endmember of this event. Hence the period ~2.2–2.0 Ga represents significant addition of both mafic and felsic material to the crust (Lu et al., 2008; Li et al., 2006).

6.1.2. $^{204}Pb/^{206}Pb$-$^{207}Pb/^{206}Pb$ (inverse Pb) and Rb—Sr isochrons provide constraints on the age of retrograde metamorphism

The inverse Pb isochron provides a robust age of 1824 ± 19 Ma (MSWD = 1), and this represents the last time that the peak metamorphic mineral assemblage was open to Pb exchange. Since this age is wholly derived from Pb, it implies that Pb has been immobile over the subsequent ~1.8 Ga. This becomes significant when considering the U—Pb and Th—Pb pseudo-isochrons, which show excess scatter due to open-system behavior between the parent elements (U and Th) and the daughter (Pb). Even though U—Pb and Th—Pb preserve ages which apparently coincide with the Rb—Sr age, significant ancient addition of U or Th to the Liaohe mafic rocks would have resulted in significant ingrowth in radiogenic Pb and hence disturbed the Pb—Pb isochron. Preservation of the Pb—Pb isochron indicates that this was not the case, and hence it is likely that any U or Th addition to the system had to occur relatively recently and the "ages" preserved by U-Th-Pb reflect closed system behavior between 1824 ± 19 Ma and a very young geologic event, very likely exposure and alteration of the rock units, which opened the isotopic systems.

Interestingly, metamorphic zircons or rims of older (2.5 or 2.2 Ga) zircons (n = 18) from the Liaohe mafic meta-igenous rocks yield a weighted average $^{207}Pb/^{206}Pb$ metamorphic age of 1896 ± 22 Ma (MSWD = 0.08; Meng et al., 2014) distinct from the whole-rock inverse Pb isochron age of 1824 ± 19 Ma from the same type of protoliths. Below we will show that the zircons and whole rocks most likely record distinct metamorphic events, peak prograde and post-peak retrograde amphibolite metamorphism respectively.

In contrast, the Rb—Sr system preserves a whole rock age of 1671 ± 58 Ma, which is significantly younger than the Pb—Pb age. Depending on the mineralogy present, whole rock Rb—Sr has long been recognized to have a significantly lower closure temperature than Pb—Pb (of the order of ~500 °C verses ~600 °C; Schaefer, 2016 and references therein) and hence it is reasonable to suggest that the Rb—Sr may simply reflect a cooling age. Whether these whole rock ages reflect uniform cooling from peak metamorphism, corresponding to <1 °C per million years, or a subsequent, distinct thermal event which completely reset the Rb—Sr (but not the Pb—Pb system) at 1671 Ma cannot be resolved by this dataset alone. $^{40}Ar/^{39}Ar$ ages of 1830–1803 Ma were obtained from amphiboles in meta-volcanic rocks (amphibolite and mafic granulite) from Ji'an, South Liaohe and Jingshan Groups in the JLJB (Faure et al., 2004; Liu et al., 2015). Such high temperature amphiboles tend to have T_c of ~540 ± 40 °C (Braun et al., 2006), slightly above that of Rb—Sr whole rock, and hence these data suggest the terrane cooled rapidly to ~540 °C by ~1.8 Ga, but remained open to Sr at ~500 °C for

the next ~130 Ma. This would suggest that the terrane remained at mid-crustal levels (25–35 km) until after ~1671 Ma.

In conclusion, we interpret the younger Rb—Sr and $^{204}Pb/^{206}Pb$-$^{207}Pb/^{206}Pb$ ages compared to the Sm—Nd and Lu—Hf ages to reflect retrograde metamorphism of the Liaohe mafic meta-igneous rocks. This interpretation implies that the isotopic composition of Sr and Pb was rehomogenized during metamorphism, but that the rocks remained largely closed systems until recently.

6.2. Geochemical Implications for the Tectonic Setting in which the Liaohe Meta-igneous Rocks Originated

Based on the metamorphic mineral assemblages and the major element chemistry, the protoliths of the amphibolites and hornblendites were most likely mafic (basaltic to andesitic) rocks (lavas or dikes) and the protolith of the metagrabbro was a gabbroic rock, representing the intrusive equivalent of the basaltic protoliths. The Liaohe amphibolites and metagabbro samples have compositions similar to modern-day mafic calc-alkaline volcanic rocks from active continental margins, for example Central America (e.g. Sadofsky et al., 2009; Heydoloph et al., 2012), Kamchatka (Duggen et al., 2007; Portnyagin et al., 2007) and Chile (e.g. Jacques et al., 2013), although they extend to more mafic compositions. The more mafic compositions are likely to reflect greater degrees of melting in a hotter Neoarchaean to Palaeoproterzoic mantle. The distinct composition of amphibolite sample LH05–14-7 compared to the other amphibolites (having the highest SiO_2, Al_2O_3 and K_2O and lowest MgO and CaO and second lowest FeO^t and TiO_2) suggests that the protolith for this sample was more evolved and had a more K-rich (high-K) calc-alkaline type composition compared to the protoliths of the other samples (Table 1; Fig. 7).

The high-grade hornblendite samples have distinct major element contents compared to the medium-grade amphibolite and metagabbro samples. The positive correlation between MgO and SiO_2 is not consistent with a link between the amphibolites and hornblendites through differentiation. The lower SiO_2 and CaO but higher FeO^t and TiO_2 in the hornblendites compared to the amphibolites are consistent with a greater abundance of hornblende (90% versus 50–60%) compared to plagioclase (10% versus 40–50%) (Table 1). The lower MgO in the higher-grade metamorphosed hornblendites with greater hornblende to plagioclase ratio, however, is unexpected and either reflects less magnesium-rich hornblende in the hornblendites or may reflect a lower MgO content in the protoliths of the hornblendites than in the amphibolites and metagabbro (Table 1). Finally, the anthophyllite-rich rock must have had an ultramafic (possibly pyroxenitic) protolith, also consistent with the lower abundances of most incompatible elements.

The patterns on the incompatible multi-element diagram (Fig. 3) for the Liaohe mafic meta-igneous rocks point to a subduction zone origin for all of the samples, as reflected by pronounced negative troughs in Nb and Ta relative to neighboring elements and general enrichment in fluid-mobile elements (Cs, Rb, Ba, U, K, Pb and Sr) and Th (Fig. 3). Elements that are fluid mobile in subduction systems can also be mobilized by fluids in the crust, so we must be cautious in using these elements for petrogenetic interpretations. Nevertheless, the incompatible element patterns in general are very similar for the different samples. Only the absolute concentrations vary, reflecting concentration or dilution of the incompatible elements as a group as a result of differentiation or accumulation processes.

To minimize problems with post-emplacement mobilization of elements, we now look at fluid-immobile-element discrimination diagrams to distinguish the tectonic setting in which the protoliths formed. Elements that are highly resistant to alteration processes include lightly compatible transition trace elements, such as Co, and incompatible elements, in particular the middle (M) and heavy (H) rare earth elements (REE), e.g., Nd, Sm, Tb, Yb, and high field strength elements (HFSE), e.g., Nb, Ta, Zr, and Ti, and Y, and Th. Since SiO_2 and the alkalis (Na_2O and K_2O) are very mobile during alteration and metamorphism, we use the Nb/Y versus Zr/Ti diagram (Fig. 7A; e.g., Pearce, 1996) as an immobile proxy for the TAS (total SiO_2 vs. alkali) diagram, to assess the nature of the protoliths for the Liaohe mafic meta-igneous rocks. All the samples plot within the basalt to basaltic andesite field, consistent with their major element compositions. In order to distinguish between a mid-ocean ridge and subduction-zone origin, we use the Nb/Yb versus Th/Yb diagram after Pearce (2008), which is capable of distinguishing MORB, intraplate or ocean island basalt (OIB) and volcanic arc basalts (Fig. 7B). All samples have elevated Th/Yb for their Nb/Yb ratios and plot within the range of volcanic arc samples. On an earlier version of this diagram, Ta/Yb versus Th/Yb, Pearce (1982) distinguishes between oceanic and active continental margin basalts and between tholeiitic, calc-alkaline, medium- and high-K calc-alkaline and shoshonitic arc rocks (Fig. 7C). Most of the Liaohe samples plot within the active continental margin calc-alkaline field, except sample LH05-14-7 with Th/Yb ratio of 7.1. This sample plots in the high-K calc-alkaline field, consistent with its high K_2O content and enriched incompatible trace element composition (see Fig. 3). In order to further test the nature of the Liaohe mafic meta-igneous rocks, we use the Co versus Th diagram after Hastie et al. (2007), considered to be an immobile proxy for the SiO_2 vs K_2O diagram (Fig. 7D), also used to discriminate between the tholeiitic, calc-alkaline and high-K calc-alkaline/shoshonite series. Co is considered to be an even better proxy for SiO_2 than Zr/Ti (Hastie et al., 2007). The Liaohe samples plot within the calc-alkaline field except LH05-14-7, which again plots in the high-K calc-alkaline/shoshonite field, which agrees well with the Ta/Yb versus Th/Yb diagram and major element chemistry.

As noted by Pearce (2008), the classification diagrams need to be applied with caution to Archaean rocks and to rocks that have been metamorphosed above low-grade amphibolite facies. Nevertheless, we believe that the general consistency between the incompatible multi-element patterns and immobile incompatible element discrimination diagrams provide us with an accurate picture of the origin of their protoliths, despite amphibolite facies metamorphism of the studied rocks. In summary, the Liaohe meta-mafic/ultramafic rocks have chemical characteristics consistent with being derived from primarily calc-alkaline basaltic protoliths formed in an active continental margin setting.

Alternative hypotheses for explaining the incompatible trace element abundances in the basalts include large amounts of crustal assimilation by upper mantle E-MORB type basalts, for example during continental rifting, or by flood basalt (Large Igneous Province = LIP) melts with relatively flat incompatible element abundances. Trondjemite-tonalite-granodiorite (TTG) crustal rocks with ages of 2.9–2.7 Ga were present in the Jiaobei Terrane of the JLJB in eastern Shandong when the Liaohe mafic and ultramafic rocks formed (An, 1990; Wang and Yan, 1992; Tang et al., 2007; Zhou et al., 2008a, b; Liu et al., 2013a, b), providing further evidence for the presence of continental lithosphere. These TTG crustal rocks formed during stabilization of the lithospheric mantle as recorded by the Sm/Nd isochron of 2.83 ± 0.18 Ga. The TTG gneisses have very high SiO_2 but low MgO, FeO^t, CaO and TiO_2 contents. As noted above, the Liaohe amphibolites and metagabbro samples have compositions similar to modern-day mafic calc-alkaline volcanic rocks from active continental margins, for example Central America (e.g. Sadofsky et al., 2009; Heydolph et al., 2012), Kamchatka (Duggen et al., 2007; Portnyagin et al., 2007) and Chile (e.g. Jacques et al., 2013). In the aforementioned studies, the authors conclude that the data allow only very minor crustal contamination. Large amounts of assimilation of crust, which would be required to generate the incompatible-element abundances, would have shifted the composition of the Liaohe mafic meta-igneous rocks towards andesitic to rhyolitic compositions and also have resulted in dramatically lower $\varepsilon Nd_{(i)}$ values than observed. Therefore, large amounts of crustal assimilation are not consistent with the mafic and ultramafic compositions of the studied samples.

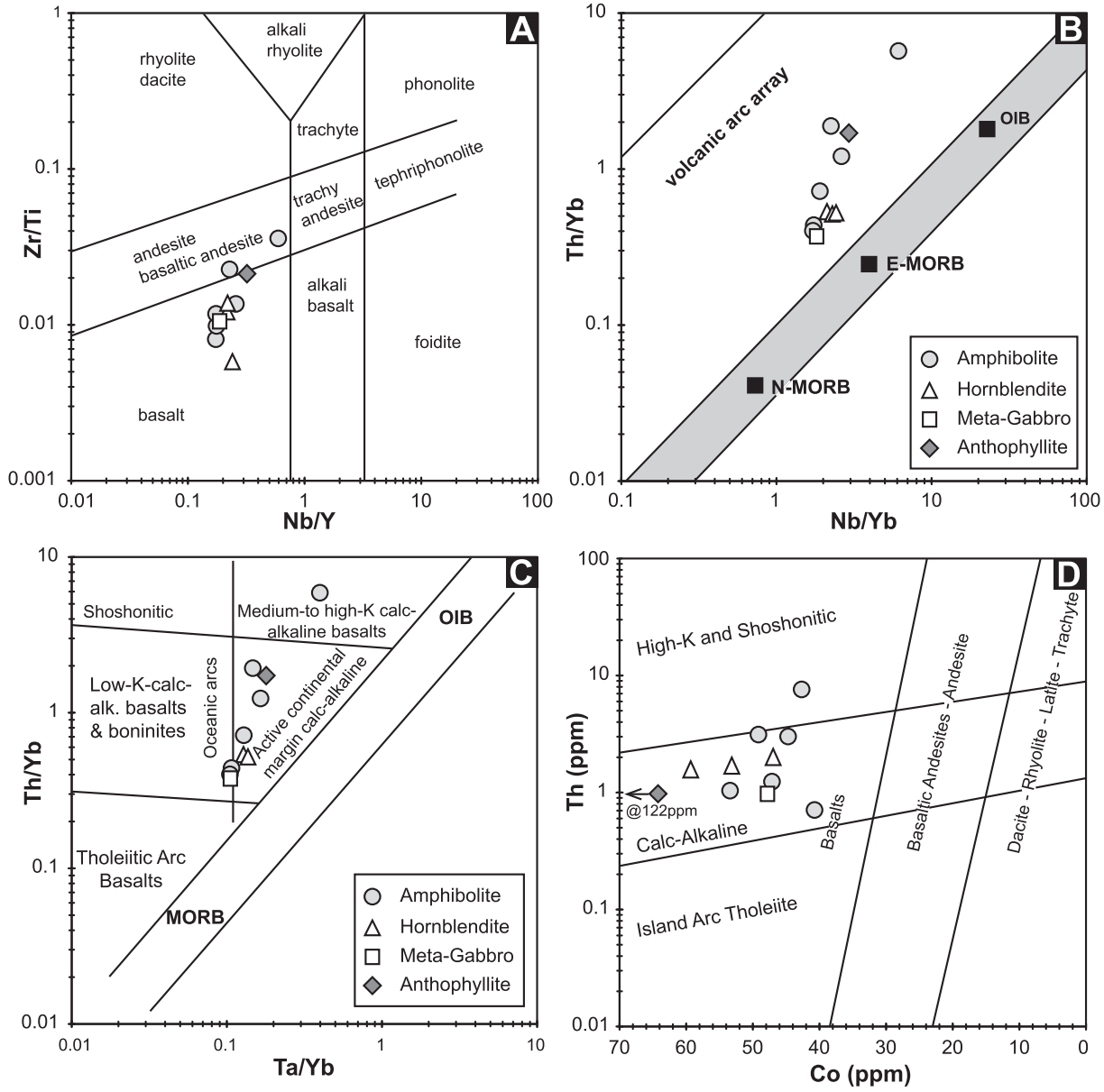

Fig. 7. Classification diagrams of a) Nb/Y versus Zr/Ti modified from Pearce (1996), b) Nb/Yb versus Th/Yb from Pearce (2008), c) Ta/Yb versus Th/Yb modified from Pearce (1992), and d) Co versus Th modified from Hastie et al. (2007). Abbreviations: N-MORB = normal mid-ocean-ridge basalt, E-MORB = enriched mid-ocean-ridge basalt, OIB = ocean island basalt, alk. = alkaline.

The positive initial εNd values (1.5–6.4) calculated for all samples at 2.83 Ga indicate that the Liaohe samples were derived from a long-term depleted source, relative to the Chondritic Uniform Reservoir (CHUR). There is no correlation between initial $\varepsilon Nd_{(2.83\ Ga)}$ or Sm/Nd and indicators of crystal fractionation (e.g. MgO, SiO_2, Ni, Zr, Nb/Yb), which usually occurs in conjunction with assimilation (DePaolo, 1981). We also note a similar range in initial εNd for ~2.7 Ga rocks from Abitibi, Canada (Blichert-Toft and Puchtel, 2010) and the Gadwal, India (Khanna et al., 2014), where assimilation of continental crust is believed to have played no more than a minor role. In summary, we do not find any evidence in support of significant crustal assimilation in the Liaohe mafic and ultramafic metamorphic rocks, implying that at least the immobile incompatible element ratios reflect the composition of the mantle melts and not major interaction between crust and mantle. The presence of older TTG rocks, together with the Sm—Nd lithospheric mantle stabilization age, provides further evidence that the Liaohe mafic meta-igneous rocks were formed in an active continental margin setting. In conclusion, we note that Faure et al. (2004) came to a similar conclusion based on the trace element geochemistry of what they describe as gabbro and pyroxenite samples from the North Liaohe Group.

6.3. Temporal and geochemical evolution of the Jiao-Liao-Ji Belt

The lithospheric stabilization, emplacement and metamorphic ages that we have determined on the Liaohe mafic meta-igenous rocks are consistent with other geochemical and age data from the JLJB. Below we review the Neoarchean through Paleoproterozoic history of the JLJB (>2.8–1.7 Ga) using literature data combined with our new data.

As mentioned above, the JLJB can be subdivided into a northern belt, including the Fenzishan, North Liaohe and Laoling groups, and a southern belt, consisting of the Wuhe, Jingshan, South Liaohe and Ji'an groups (going from southwest to northeast). Detrital zircons in metasediments from the Jiaobei Terrane (southwestern JLJB), the South Liaohe Group (central JLJB) and the Ji'an and Laoling groups

(northeastern JLJB) record nearly continuous magmatism (on a scale of <100 Ma) from 3.6 to 2.0 Ga (Luo et al., 2004; Wan et al., 2006; Zhou et al., 2008a, b; Liu et al., 2013a, b; Wang et al., 2017; Zhang et al., 2018; Liu et al., 2015, 2019b). Such detrital zircon records are heavily weighted towards intermediate to felsic magmatism as mafic and ultramafic lithologies produce a paucity of zircons available to be eroded.

Considerable age and geochemical data are available from the Jiaobei (Jiaodong) Terrane from magmatic and metamorphic zircons. Magmatic zircons are characterized by low luminescence, often show zoning, and high Th/U ratios, whereas metamorphic zircons and zircon rims show nebulous zoning or are structureless, have high luminescence and relatively low Th/U ratios. SHRIMP and LA-ICP-MS zircon U—Pb analyses from supracrustal rocks and granitoid gneisses in the Jiaobei Terrane record three magmatic events between 2.9 and 2.5 Ga, taking place at ~2.9, ~2.8–2.7 and ~ 2.55 Ga (Tang et al., 2007; Jahn et al., 2008; Zhou et al., 2008b; Liu et al., 2013a, b; Wu et al., 2014).

Mafic meta-igneous lenses, enclaves and blocks, probably representing parts of stretched and thinned dikes, in the Archean TTG gneisses of the Jiaobei Massif produce similar and younger ages than the TTG gneisses. A mafic granulite sample yielded SHRIMP $^{207}Pb/^{206}Pb$ zircon weighted mean ages of 2638 ± 22 Ma, interpreted as the crystallization age of the mafic igneous protolith of the granulite sample, and 2703 ± 12 Ma, interpreted as the crystallization age of xenocrystic zircons in the protolith derived from the underlying basement (Tam et al., 2011). Magmatic zircons from the supracrustal amphibolites in the Jiaobei Terrane yielded weighted mean concordant U—Pb zircon ages of 2.59–2.50 Ga, interpreted as the crystallization ages of the mafic magmatic protoliths (Zhang et al., 2003; Tang et al., 2007; Wu et al., 2014). Xenocrystic U—Pb zircon ages in mafic meta-igneous rocks from the Liaohe Group range from 2.55 to 2.46 Ma and largely overlap ages of the younger amphibolites in the Jiaobei Massif (Meng et al., 2014; Xu et al., 2020). Finally, a mafic granulite from the Jiaobei Terrane yielded a LA-ICP-MS weighted mean $^{207}Pb/^{206}Pb$ zircon crystallization age of 2379 ± 54 Ma (Tang et al., 2007). In conclusion, the magmatic zircon age data provide evidence that mafic magmatism took place at least from ~2.7–2.5 Ga (Tang et al., 2007; Meng et al. 2014), overlapping with the younger end of TTG formation in the JLJB (Lu et al., 2008).

Geochemical data is sparse from these mafic meta-igneous rocks. An amphibolite (03SD06) in the Jiaobei TTG gneisses, which produced a weighted mean $^{207}Pb/^{206}Pb$ zircon age of 2506 ± 18 Ma interpreted to be the crystallization age of a mantle-derived mafic dike, however, has subduction-type geochemical characteristics, e.g. Nb depletion relative to Th and La (Tang et al., 2007). Hf model ages from the magmatic zircons in the Jiaobei Terrane range from 3.9 to 2.6 Ga with a major peak at 3.4–3.1 Ga and a subordinate peak at 2.8–2.7 Ga (Wu et al., 2014). The Hf isotopes point to major juvenile crustal growth with substantial additions of older crust between 3.4 and 3.1 Ga and 2.8–2.7 Ga and crustal reworking with minor juvenal addition at ~2.55 Ga (Wu et al., 2014). The younger ~2.55 Ga episode of granitoid formation presumably resulted primarily from remelting of the ~2.8–2.7 Ga juvenile crust. The sparse geochemical data available for these older mafic meta-igneous rocks are consistent with formation in a subduction zone.

Our 2.83 ± 0.18 Ga lithospheric stabilization (Sm—Nd whole rock) isochron for Liaohe mafic meta-igenous rocks provides evidence of the complementary mantle contribution to the 2.8–2.7 Ga crustal evolution in the Jiaodong Terrane (e.g. Liu et al., 2013a, b), and reflects the timing of final melt extraction and possibly ultimate cratonization of the SCLM beneath this terrane. Rocks with ages >3 Ga are rare in the Eastern Block of the North China Craton but are found in the Anshan Domain north of the Liaohe Group (~3.8–2.5 Ga; Song et al., 1996; Wan et al., 2005; Lu et al., 2006; Wu et al., 2014), suggesting that the studied igneous rocks were formed on basement of the former Longgang Block (northwestern part of the present Eastern Block).

Abundant evidence exists that mafic and granitic magmatism took place between ~2.25–2.00 Ga in the central JLJB. In one of the earliest studies, zircons from a granite in the South Liaohe Group (also called the Kuandian Complex) in eastern Liaoning Province produced a minimum upper intercept U—Pb age of 2.14 ± 0.05 Ga, whereas whole rock Nd isotope data point to an age between 2.4 and 2.3 Ga for granite and amphibolite rocks (Sun et al., 1993). The authors interpreted the granites to be derived from the amphibolite protoliths (basalts) through fractional crystallization with little to no crustal assimilation based on the Nd isotope ratios and REE abundances. In the absence of crustal assimilation, the MORB normalized (Th, Ce)/(Nb, Ta) ratios >1 in the amphibolites (estimated from Fig. 4 in Sun et al., 1993) point to a subduction zone origin rather than through intraplate (continental flood basalt) volcanism as proposed by the authors. A subduction-zone origin is also consistent with the high fluid-mobile-element (Sr, K, Rb, Ba) and Th contents.

A compilation of U—Pb zircon ages (267) from 17 Liaohe mafic samples from the Liaodong Peninsula give an age range of ~2.25–2.02 Ga with a peak of activity at 2.12–5 Ga (Xu et al., 2020). SHRIMP and LA-ICP-MS U—Pb zircon ages for the Liaoji Granitoids (North and South Liaohe Groups), monzogranitic geneisses from the Jiaobei Terrane, and syenogranites from the Jilin Province yield a very similar range in crystallization ages of ~2.25–2.00 Ga (Li et al., 2003, 2006; Lu et al. 2004a, b, 2006; Luo et al. 2004, 2008; Wan et al., 2006; Li and Zhao, 2007; Liu et al., 2013a, b; Meng et al., 2014; Xu et al., 2018a, b). U—Pb zircon ages (88) from four felsic tuffs from the Liaodong Peninsula primarily fall within the range of 2.3–2.1 Ga with a peak at 2.17 Ga (Xu et al., 2020). It is therefore reasonable that the mafic meta-igneous rocks investigated here were part of this magmatic event, and indeed represent the mafic end member of subduction-zone magmatism active during this time. In conclusion, we interpret the mafic rocks to have been derived from a lithospheric mantle source, which was isolated at 2.83 ± 0.18 Ga (Sm—Nd isochron), which was part of a convergent margin when the mafic magmas formed at 2.25 ± 0.31 Ga (Lu—Hf isochron).

Now we will review the geochemical data for the Jiaobei Terrrane and Liaohe Group mafic meta-igneous rocks. Liu et al. (2013a, b) suggest that the crustal reworking at ~2.5 Ga resulted from magma underplating by upwelling plumes. Granitoid formation as a result of plume-related underplating applies well to the Taishan area in western Shandong Province, where ~2.7 Ga greenschist to amphibolite facies komatiitic and tholeiitic basalts are associated with a ~ 2.5–2.7 Ga TTG and supracrustal sequence (Wang et al., 2013). When comparing the Jiaobei (Tang et al., 2007) and Liaohe mafic meta-igenous rocks with similar-aged komatiitic and tholeiitic basalts from the Taishan area in western Shandong Province (Wang et al., 2013), the difference in origin can be demonstrated in highly immobile incompatible element ratios, such as Nb/La (0.71–1.61 in the Taishan mafic volcanics versus 0.04–0.98 in the Jiaobei and Liaohe mafic meta-igneous rocks), Nb/Th (7.25–23.75 versus 0.22–4.56, respectively) and Th/Yb (0.05–0.60 versus 0.40–7.12, respectively). Low Nb/La, Nb/Th and high Th/Yb are source characteristics transferred into the resulting subduction zone mafic magmatism. The compositions of the mafic Liaohe rocks in the JLJB overlap with modern-day mafic arc igneous rocks, providing strong support that they formed in a subduction-zone environment. Excluding one sample, the initial $\varepsilon Nd_{(i)}$ of the Jiaobei amphibolites show depleted (+3.4 − +5.7) mantle source compositions (Tang et al., 2007), similar to the Liaohe mafic/ultramafic meta-igneous rocks (εNd = +1.5 − +6.4). The zircons also yield normal mantle O isotope compositions for these samples (Tang et al., 2007). In conclusion, there is no evidence for plume-related magmatism between ~2.6–2.0 Ga in the JLJB, but rather for subduction-related magmatism.

Thousands of metamorphic zircons or zircon rims have been dated from the JLJB. An older metamorphic episode has been recorded in mafic meta-igneous rocks from the Jiaobei Terrane following the 2.55 Ga magmatic event. Wu et al. (2014), for example, report mean weighted $^{207}Pb/^{206}Pb$ metamorphic ages of 2.52–2.46 Ga in amphibolites and granitoids and an apparent $^{207}Pb/^{206}Pb$ age of 2.4 Ga in a biotite-plagioclase gneiss. Most U—Pb ages from

metamorphic zircons and rims from the JLJB, however, range from ~1.97–1.73 Ga (e.g. Zhao et al., 2012; Wu et al., 2014; Liu et al., 2015, 2019b). The granulite-facies metamorphic evolution of the northern (including Fenzishan, North Liaohe and Laoling groups) and southern (including Jingshan, South Liaohe and Ji'an groups) zones of the JLJB were believed to be distinct with the northern zone undergoing a clockwise P-T-t (pressure-temperature-time) path and the southern zone an anti-clockwise path (Lu, 1996; Lu et al., 1996; He and Ye, 1998; Li et al., 2001b; Zhao et al., 2012), but recently it has been demonstrated that the southern, like the northern, zone also underwent a clockwise P-T-t path (see Liu et al., 2019a, b and references therein). Mineral inclusions in dated zircons indicate that peak granulite-facies metamorphism took place at ~1.94–1.89 Ga along the entire JLJB (including the North and South Liaohe Group rocks and the Liaoji Granitoids in the central JLJB, the Jingshan Group in the southern JLJB, and the Ji'an and Laoling Groups in the northeastern JLJB), which is interpreted to reflect collision of the Nangrim with the Longgang Block (Luo et al. 2004, 2008; Li et al., 2005a, 2005b; Lu et al., 2006; Wan et al., 2006; Li and Zhao, 2007; Tam et al., 2011, 2012a, b, c; Wu et al., 2014; Wang et al., 2017; Zhang et al., 2018; Liu et al., 2019a, b). Specifically, the metamorphic zircons and rims from the Liaohe mafic meta-igneous rocks (with an age range of 1.92–1.87 Ga and a peak at 1.90 Ma; Meng et al., 2014) demonstrate that these rocks underwent this metamorphic event, recorded along the entire JLJB.

Inclusions in dated metamorphic zircons from meta-sedimentary and meta-mafic/ultramafic rocks throughout the JLJB indicate that retrograde metamorphism took place from ~1.88 to <1.73 Ga (Lu et al., 2006; Zhao et al., 2006b; Zhou et al., 2008a; Tam et al., 2011; Wu et al., 2014; Liu et al., 2019a, b). Felsic magmatism, including intrusion of porphyritic monzogranites, granites and syenogranites, also took place throughout the JLJB between 1.88 and 1.80 Ga in an anorogenic or post-tectonic extensional setting (Cai et al., 2002; Li et al., 2004; Lu et al., 2004a,b, 2006; Zhai et al., 2005; Li and Zhao, 2007; Tam et al., 2011; Liu et al., 2013a, b). Porphyritic monzogranites with similar ages (1.87–1.84 Ga) occur in North and South Korea within both the Nangrim Block and the Imjingang Belt, suggesting that this was a large-scale event that occurred after the collision of the Nangrim Block with the Longgang Block (Zhao et al., 2006a, b; Kim et al., 1999; Zhai et al., 2005; Kim and Cho, 2003; Lee et al., 2005). Migmatites cover >1100 km of the southern zone of the JLJB, extending from the Jingshan Group on the Jiaodong Peninsula in the south, through the South Liaohe Group on the Liaodong Peninsula to the Ji'an Group in south Jilin (Liu et al., 2019b). Anatectic zircons in granitic leucosomes, widespread in the migmatites, show that extensive partial melting took place during a similar time interval of ~1.88–1.80 Ga (Liu et al., 2013b, 2019a, b). Together the felsic magmatism and partial melting to form the migmatites and granitic leucosomes resulted from exhumation, due to extension and thinning, of the JLJB related to the post-peak MP-LP granulite facies retrograde metamorphism with a near isothermal decompression P-T path occurring at 1.87-1.84 Ga along the JLJB and between 1.85 and 1.84 Ga in the South Liaohe Group (Liu et al., 2015, 2019b). Thereafter an amphibolite facies retrogression took place between 1.83 and 1.80 Ga (e.g. Liu et al., 2015, 2019b), for example recorded in the four amphibolite samples investigated by Wu et al. (2014), which yielded $^{207}Pb/^{206}Pb$ metamorphic ages of 1854 ± 12, 1838 ± 25, 1836 ± 73 and 1823 ± 41 and 1808 ± 27 Ma. These ages are within error of our whole rock $^{207}Pb/^{206}Pb$ age of 1824 ± 19 Ma for the Liaohe mafic (amphibole-bearing) meta-igneous rocks (amphibolites, hornblendites and metagabbro). Therefore, it is apparent that the terrane was subject to an elevated geotherm for an extended period of time after peak orogenesis, cooling through the Pb—Pb closure temperature of ~600 °C by 1824 Ma and soon after through the Ar—Ar hornblende closure temperature of ~540 °C at 1800 ± 10 (Faure et al., 2004). The terrane did however remain at mid-crustal depths above the ~500 °C closure temperature of Rb—Sr until ~1671 ± 58 Ma.

In summary, dating of detrital zircons shows that crustal formation in the JLJB extends back to ≥3.6 Ga, whereas direct dating of meta-igneous rocks shows that the lithospheric mantle became isolated and presumably stabilized between ~3.0–2.6 Ga based on our whole-rock mafic Lioahe meta-igneous Sm—Nd age (2.83 ± 0.18 Ga). Felsic magmatism at ~2.55 Ga, was predominantly generated by remelting of ~2.8–2.7 Ga TTG (Jahn et al., 2008) and supracrustal rocks, but some juvenile mafic magmas with calc-alkaline (subduction-related) compositions were also produced during this event (Tang et al., 2007). Subsequent mafic volcanism at ~2.25–2.02 Ga in the Liaohe Group also shows subduction-related geochemical characteristics (Lu et al., 2006; Li and Zhao, 2007). This complete package, including supracrustal sedimentary sequences, experienced prograde collision-related metamorphism between ~1.96–1.88 Ga, whereas retrograde post-tectonic metamorphism (extension, cooling and exhumation) and anorogenic magmatism commenced between ~1.88-1.80 Ga, passing through Pb-Pb whole-rock, Ar-Ar hornblende and Rb-Sr whole-rock closure temperatures at 1824 ± 19, 1800 ± 10 and 1671 ± 58 Ma respectively.

6.4. Model for the evolution of the Jiao-Liao-Ji Belt from ~2.8 to 1.7 Ga

Results of this study, in conjunction with those from previously published lithological, structural, geochemical and geochronological studies, enable us to place constraints on the evolution of the JLJB. We will begin by reviewing existing models and then will propose a new model integrating our new whole rock data with published whole rock and zircon data. The existing models for the origin and evolution of the JLJB can be divided into two endmember groups (e.g. see summary by Zhao and Zhai, 2013): 1) opening and closing of an intracontinental rift (e.g., Zhang and Yang, 1988; Peng and Palmer, 1995; Li et al., 2004, 2005a, 2005b, 2006; Luo et al., 2004, 2008; Li and Zhao, 2007) and 2) arc (island arc or active continental margin) - continent collision (e.g., Bai, 1993; Bai and Dai, 1998; He and Ye, 1998; Faure et al., 2004; Lu et al., 2006; Li et al., 2018; Xu et al., 2018a, b).

Rift-related models propose that the Longgang and Nangrim (= Langrim = Langling) Blocks originally formed a single continental block that was rifted apart in the early Paleoproterozoic (2.2–1.9 Ga), accompanied by deposition of sedimentary and volcanic rocks into the rift basin and intrusion of mafic and granitoid rocks along rift-related faults. Closure of the rift in the late Paleoproterozoic resulted in the formation of the Jiao-Liao-Ji Belt (Yang et al., 1988; Zhang and Yang, 1988; Zhang et al., 1988; Li et al., 2001a, 2001b, 2004, 2005a, 2006, 2012). Zhao and Zhai (2013) argue that the following lines of evidence support this model: (1) bimodal volcanic suites in the JLJB, including meta-mafic volcanic rocks (greenschists and amphibolites) and meta-rhyolites (Zhang and Yang, 1988; Sun et al., 1993; Peng and Palmer, 1995); (2) large volumes of A-type granites in the JLJB (e.g. Li and Zhao, 2007); (3) low-pressure, anticlockwise, P-T paths of the Ji'an, South Liaohe and Jingshan Groups (Lu, 1996; Lu et al., 1996; He and Ye, 1998b; Li et al., 2001b), which are not consistent with arc- or continent-continent collision, and (4) non-marine borate deposits in the JLJB with similarities to borate-bearing successions in other Proterozoic rifting environments (Jiang, 1987; Peng et al., 1998). Problems with the rift model are explaining 1) what triggered its closing and the deformation event at ~1.96–1.88 Ga, 2) the high-pressure, clockwise P-T-t paths found in both the northern (Fenzishan, North Liaohe and Laoling) and more recently also in the southern zone of the JLJB (e.g. Jingshan, South Liaohe and Ji'an groups; Liu et al., 2019a, b), showing that the anti-clockwise paths were incorrect, and 3) the origin of high-pressure pelitic rocks that require subduction or continental collision to get them to sufficient depths to undergo high pressure metamorphism (e.g. Zhao and Zhai, 2013; Liu et al., 2019a), and 4) the presence of mafic meta-igneous rocks with subduction-related geochemistry (Faure et al., 2004; Meng et al., 2014; Xu et al., 2018a,b, 2020; Xu et al., 2020; this study).

The second group of models argue for arc (island arc or active continental margin) - continent collision (e.g. Bai, 1993; Bai and Dai, 1998; He and Ye, 1998; Faure et al., 2004; Lu et al., 2006; Li et al., 2018). Bai (1993), the first to argue that arc-continent collision formed the JLJB, proposed that the Liaonan-Nangrim Block was an island arc and the Liaohe Group a back-arc basin. Collision of this arc system with the Archean Longgang Block caused the closure of the back-arc basin and formation of the JLJB in the Paleoproterozoic. Faure et al. (2004) showed that the mafic/ultramafic meta-igenous rocks have incompatible-element characteristics similar to continental arcs and proposed that subduction was beneath the southern Palaeoproterozoic (Nangrim) continental block and that it was thrust upon the Anshan Block when the two blocks collided. Other variations of the arc-continent collisional model have also been proposed (e.g. Bai and Dai, 1998; He and Ye, 1998; Lu et al., 2006) with the most recent models favoring subduction of the Nangrim Block northwestwards beneath the Longgang active continental margin Block (e.g. Wang et al., 2017; Xu et al., 2018b; Zhang et al., 2018). Meta-sediments in the JLJB have been interpreted as having formed in the forearc and passive margin of the Nangrim Block (e.g. South Liaohe Group; Wang et al., 2017) or in a backarc basin (e.g. North Liaohe group; Wang et al., 2017; Ji'an and Laoling groups; Zhang et al., 2018). The mafic Liaohe meta-igneous rocks have been interpreted by some to have EMORB type compositions and thus it has been argued that they formed in a backarc basin floored by oceanic crust (Tang et al., 2007; Meng et al., 2014). The absence of an ophiolite associated with the JLJB, however, is not consistent with a backarc basin floored by ocean crust, since closure of back-arc basins floored by ocean crust generally result in obduction (rather than subduction) of the seafloor. We note that non-marine borate deposits could have formed in a backarc rift setting that had not progressed to becoming a marine backarc basin. Finally, the geochemical data from mafic meta-igneous rocks in the JLJB point to them having been formed as part of a magmatic arc (active continental margin; e.g. Faure et al., 2004 and this study) rather than in a back-arc basin setting.

We now review our whole rock data combined with published results from whole rocks and zircons to present an integrated model for the evolution of the JLJB from ~2.8–1.7 Ga. As summarized above, U—Pb zircon age data from detrital zircons in supracrustal rocks (3.6–2.0 Ga), TTG gneisses (2.9–2.5 Ga) and mafic meta-igneous rocks from the Liaohe and the Jiaobei Terranes (2.7–2.5 Ga) provide direct evidence that Neoarchaean crust exists beneath the Liaohe Group and Liaoje granitic rocks and/or that the JLJB crust was located adjacent to crust with these ages (Tang et al., 2007; Jahn et al., 2008; Zhou et al., 2008b; Liu et al., 2013a, b; Wu et al., 2014; Zhang et al., 2018; Liu et al., 2015, 2019b). The Hf model ages from the zircons in the Jiaobei Terrane extend as far back as 3.9 Ga and show major juvenile crustal growth between 3.4 and 3.1 Ga and 2.8–2.7 Ga and crustal reworking with minor juvenal addition at ~2.5 Ga (Wu et al., 2014). Our Sm—Nd lithospheric mantle age of 2.8 ± 0.2 Ga from the mafic meta-igneous rocks from the Liaohe Group points to lithospheric mantle stabilization (cratonization) between ~3.0–2.6 Ga (Fig. 8A). Unfortunately, there is little geochemical data available from the mafic samples with ages ≥2.3 Ga, which provides information about the petrogenesis of these rocks. An amphibolite sample dated at 2.50 Ga, however, shows a subduction-type geochemical signature, suggesting that subduction took place at this time (Tang et al., 2007) and may have caused the crustal reworking. Lithospheric stabilization taking place at 2.8 ± 0.2 Ga argues against a significant role for mantle plumes and lithospheric drips (Nebel et al., 2018) in causing crustal growth between 2.9 and 2.7 Ga, because plumes and lithospheric drips would cause lithospheric mantle thinning rather than stabilization. Therefore, although speculative, we favor formation of the ~3.0–2.5 Ga crust and lithospheric mantle forming the JLJB basement through subduction.

The major phase of magmatism in the JLJB took place between 2.3 and 2.0 Ga and was subduction-related (Fig. 8B). The Liaohe mafic meta-igneous rocks were emplaced at 2.25 ± 0.31 Ga (whole rock isochron) and ~ 2.25–2.02 Ga with peak age at 2.15–2 Ga (U—Pb zircon ages; Xu et al., 2020), overlapping with the Liaoje granitoid rocks emplaced between ~2.2–2.0 Ga (e.g. Li and Zhao, 2007; Zhou et al., 2008a, b). The geochemistry of the Liaohe mafic/ultramafic meta-igneous rocks is consistent with mafic arc magmatism having formed along an active continental margin (e.g. Bai and Dai, 1998; Faure et al., 2004). An active continental margin setting is further supported by the presence of Neoarchaean supracrustal rocks and TTG gneisses in the JLJB covering the age range of 2.9–2.5 Ga (Tang et al., 2007; Jahn et al., 2008; Zhou et al., 2008a, b; Liu et al., 2013a, b; Wu et al., 2014). In addition, U—Pb ages of detrital zircons from meta-sediments along the entire JLJB record nearly continuous (on a scale of <100 Ma) intermediate to felsic magmatism and/or metamorphic events from 3.6 to 2.0 Ga (Luo et al., 2004; Wan et al., 2006; Zhou et al., 2008a, b; Liu et al., 2013a, b; Wang et al., 2017; Zhang et al., 2018; Liu et al., 2019b), and Hf model ages indicate crustal growth between 3.9 and 2.5 Ga (Wu et al., 2014). Crustal rocks with such ages have been identified in the Archaean Anshan Sequence in the Liaoning Province on the Longgang Block (3.8–2.5 Ga), which consists primarily of granitic rocks that experienced greenschist- to granulite-facies metamorphism, but not on the Nangrim Block (2.55–2.45 Ga), which consists primarily of quartz diorites and amphibolites that were exposed to amphibolite-facies metamorphism (Lu et al., 2006; Dong et al., 2017; Liu et al., 2017c; Wang et al., 2017; Liu et al., 2019a). Considering the overlap in magmatic evolution of the crust beneath the JLJB and on the Longgang Block, we place the active Paleoproterozoic (~2.3–2.0 Ga) continental margin on the southeast side of the Longgang Block rather than on northwest side of the Nangrim Block (Fig. 8B). Although it is likely that the protoliths of some of the meta-sedimentary rocks were deposited in a back-arc (as well as forearc) basin (e.g., Wang et al., 2017; Zhang et al., 2018), there is no direct evidence in the form of an ophiolite for this basin having been floored by oceanic crust formed by back-arc spreading.

The clockwise P-T-t path for the northern and southern zones of the JLJB (e.g. Liu et al., 2019a) are consistent with a collisional event having taken place between ~1.96–1.88 Ga, as seen in metamorphic zircons and zircon rims from both felsic and mafic meta-igneous rocks throughout the JLJB. Mineral assemblages in the zircons indicate that peak granulite-facies metamorphism occurred at ~1.94–1.89 Ga. This prograde metamorphic event no doubt represents collision and orogenesis between the Longgang Block and the Nangrim (micro-continental) Block to form the Eastern Block of the North China Craton (Fig. 8C). Inclusions in U—Pb dated zircons indicate that retrograde metamorphism took place between ~1.88–1.73 Ga throughout the JLJB (e.g. Liu et al., 2019a, b). Felsic magmatism and migmatites with granitic leucosomes, representing partial melting of felsic minerals (quartz and feldspars), record post-peak MP-LP granulite facies retrograde metamorphism with near isothermal decompression between 18.7 and 18.4 Ga along the JLJB, followed by an amphibolite facies retrogression between 1.83 and 1.80 Ga (e.g. Liu et al., 2015, 2019b). Our whole rock inverse Pb—Pb isochron age of 1.82 ± 0.2 Ga for the Liaohe mafic (amphibole-bearing) meta-igneous rocks records this event. This post-orogenic period is associated with regional cooling, but temperatures remained above 500 °C (at mid-crustal levels of ~25–35 km) until ~1.67 ± 0.6 Ga (Liaohe mafic meta-igneous whole-rock Rb—Sr isochron). We propose that overthickening of the lithosphere during the collisional event is likely to have resulted in lithospheric destabilization, resulting in lithospheric mantle detachment/delamination (Li and Zhao, 2007). Lithospheric mantle removal triggered orogenic collapse, causing extension and thinning, coupled with exhumation and anatexis (Fig. 8D).

Assembly of the North China Craton appears to have taken place through amalgamation of at least four micro-continental blocks via three collisional events. The Nangrim-Longgang collision described here formed the Eastern Block (Fig. 8), whereas amalgamation of the Yinshan and Ordos micro-continental blocks formed the Western Block. Assembly of these four blocks occurred contemporaneously but

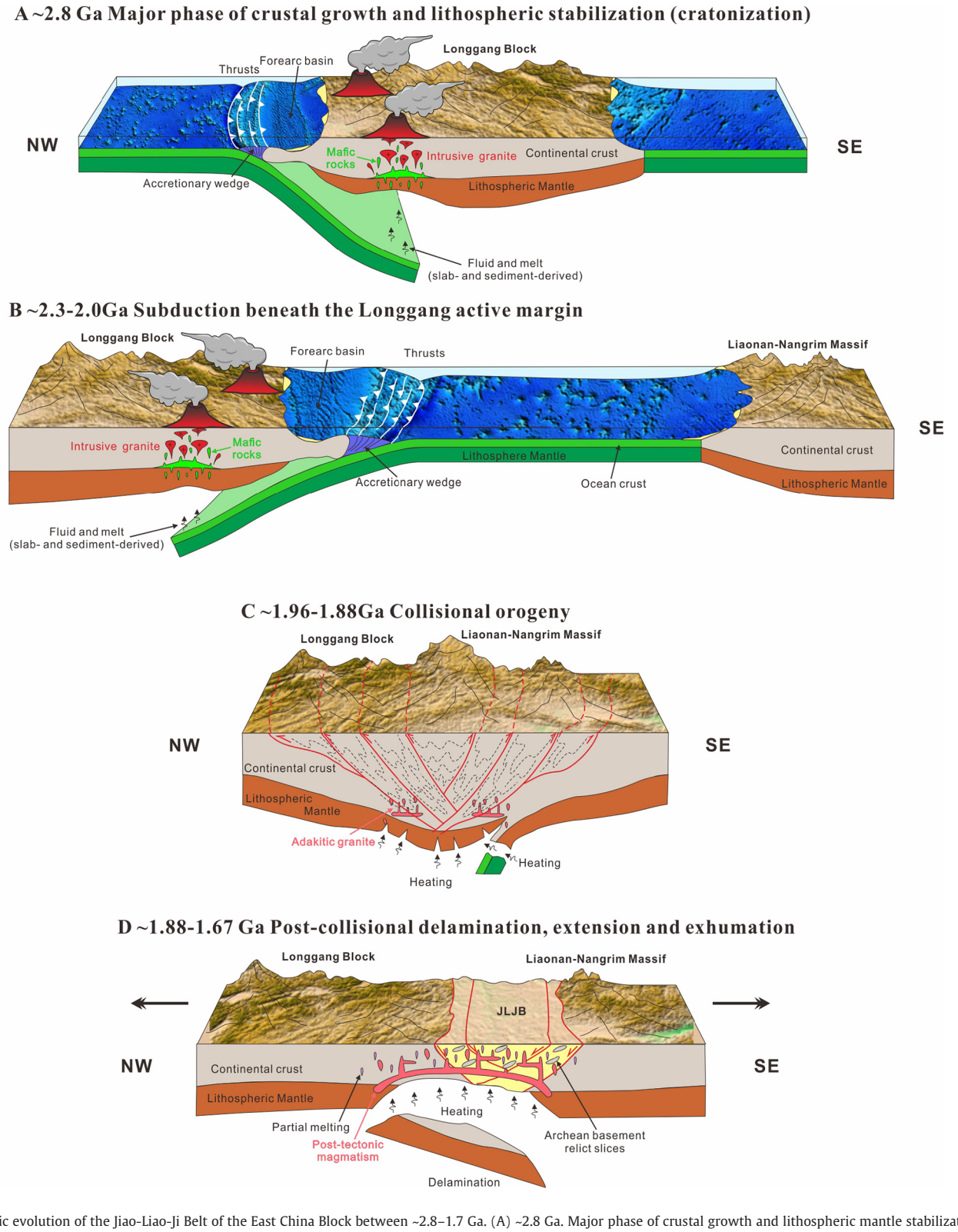

Fig. 8. Tectonic evolution of the Jiao-Liao-Ji Belt of the East China Block between ~2.8–1.7 Ga. (A) ~2.8 Ga. Major phase of crustal growth and lithospheric mantle stabilization (cratonization) beneath the Jiao-Liao-Ji Belt, North China Craton. We favor formation of crust and lithosphere through subduction processes, since mantle plumes and lithospheric dripping are likely to cause thinning of the lithospheric mantle rather than its stabilization. We show subduction but the direction of subduction is assumed. Subduction is likely to have occurred intermittently until ~2.3 Ga. (B) ~2.3–2.0 Ga. Subduction of oceanic crust attached to the Nangrim Block northwestwards beneath the active southeast continental margin on the Longgang Block. Mafic melts in the subduction zone are derived from the ~2.8 Ga lithospheric mantle. Melting results from addition of hydrous fluids/melts from the subducting oceanic crust to the lithospheric mantle beneath the southeast edge of the Longgang Block (Li et al., 2010). Granites are formed coevally and primarily by differentiation of mafic melts due to mafic magma underplating (Li et al., 2001, 2005; Li and Zhao, 2007). (C) ~1.95–1.88 Ga. Collision of the active Longgang continental margin with the passive Nangrim continental margin caused closure of the ocean basin, crustal thickening, orogenesis, and peak metamorphism up to granulite grade. (D) ~1.88–1.67 Ga. Destabilization of the thickened lithosphere resulted in delamination/detachment of the lithospheric mantle and possibly lower crust, causing extension and thinning of the lithosphere in the JLJB and orogenic collapse. Exhumation resulted in retrograde metamorphism and crustal anatexis that generated post-tectonic anorogenic granites and migmatites. MP-LP retrograde metamorphism was isothermal between ~1.87–1.84 Ga and went through the amphibolite facies between ~1.83–1.80 Ga (Liu et al., 2019a, b), which is recorded in the whole-rock inverse Pb—Pb isochron of the Liaohe mafic meta-igneous rocks. Rocks cooled from ~600 to ~500 °C between 1.82 Ga (Pb—Pb inverse isochron) and 1.67 Ga (Rb—Sr isochron).

independently at ~1.95 Ga. Collision between the Western and Eastern Blocks took place at ~1.85 Ga during the time that the JLJB rocks were undergoing isothermal retrograde metamorphism. As continental blocks became larger, thicker and more abundant in the Paleoproterozoic, collisional tectonics may have resulted in the amalgamation of many smaller blocks into cratons (Li et al., 2018), such as the North China Craton, that later were fused together through further collisions to form supercontinents such as the Meso-Paleoproterozoic Supercontinent Columbia (Zhao et al., 2002a, b; Li et al., 2019), which at some stage became unstable and broke apart only to reassemble again at a later stage (Zhao et al., 2004).

7. Conclusions

Our study of whole rock geochronology and geochemistry of mafic/ultramafic meta-igneous rocks from the Liaohe Group of the Eastern Block of the North China Craton, when interpreted in conjunction with the U—Pb and Lu—Hf zircon record, allows us to add key constraints to the evolution of Neoarchaean-Paleoproterozoic tectonics of the North China Craton. These include:

1) Mantle lithospheric stabilization took place at ~2.8 Ga beneath the Jiao-Liao-Ji Belt. This lithospheric mantle was subsequently sampled by the Liaohe mafic and ultramafic subduction-related magmas. Due to high degrees of melting, the mafic magmas preserved the Sm—Nd age of their lithospheric mantle source.
2) The geochemistry of the Liaohe mafic magmatism points to an origin along an active continental margin. Available published data from other parts of the Jiao-Liao-Ji Belt also point to a subduction origin and display similar emplacement and metamorphic ages as the Liaohe mafic meta-igneous rocks.
3) Emplacement of the Liaohe mafic and ultramafic rocks, as preserved in a whole-rock Lu—Hf isochron (2.25 ± 0.31 Ga), was likely synchronous with the formation of the Liaoje granitoids intruded between 2.2 and 2.0 Ga in an active continental margin subduction-zone setting. We place the active continental margin on the southeastern side of the Longgang Block, since Archaean supracrustal rocks and TTG gneisses from the JLJB have zircon U—Pb ages and Hf model ages (3.9–2.5 Ga), similar to ages from the Archean Anshan sequence (3.8–2.5 Ga) in the northern Liaoning Province on the Longgang Block but much older than ages found on the Nangrim Block (2.55–2.45 Ga) thus far.
4) Collision of the active Longgang continental margin with the passive Nangrim continental margin at ~1.96–1.88 Ga, as recorded in metamorphic zircons (by U—Pb age dating) from the Liaohe mafic meta-igneous rocks and felsic rocks along the entire Jiao-Liao-Ji Belt, caused orogensis and granulite-grade metamorphism.
5) Crustal thickening related to the collisional event triggered lithospheric destabilization and detachment/delamination, resulting in exhumation and retrograde metamorphism, crustal anatexis and generation of a post-tectonic anorogenic granites at ~1.88–1.80 Ga, recorded in the mafic meta-igneous rocks (whole-rock Pb—Pb age of 1.82 ± 0.02 Ga) and metamorphic zircons (U—Pb) throughout the Jiao-Liao-Ji Belt. Cooling due to exhumation reached a temperature of ≤500 °C at ~1.67 ± 0.06 Ga, based on the Rb—Sr whole rock isochron.

In conclusion, whole-rock isotopic analysis of mafic lithologies enables extension of the zircon geochronological record to include the age of lithospheric mantle stabilization (Sm—Nd), the timing of mafic magmatism (Lu—Hf), consistent with zircon age data from similar mafic meta-igneous Liaohe rocks, exhumation and retrograde amphibolite metamorphism (Pb—Pb), and constraints on post-orogenic cooling (Rb—Sr, U—Pb and Th—Pb).

Credit author statement

KH wrote the manuscript with significant input from BS and SL. SL carried out field work to collect samples. FH carried out the isotope analyses and contributed to the manuscript text. XL contributed to the interpretations in the manuscript. DG-S carried out the ICP-MS analyses. RZ contributed to the interpretations in the manuscript. YL contributed to development of the model and drafted the model figure.

Declaration of competing interest

The authors declare that they have no known competing financial interests or personal relationships that could have appeared to influence the work reported in this paper.

Acknowledgements

This research was funded by the NSFC project (China) to SL (Grants 91958214, 41325009, 41072152 and 41190072) and by the Leibniz and Helmholtz Societies (Germany). The research was initiated by a visit of Prof. Dr. Sanzhong Li to GEOMAR in 2007 and concluded during a sabbatical by Prof. Dr. Bruce Schaefer to GEOMAR in 2019, which was funded by Macquarie University (Australia).

Appendix A. Appendix

A.1. Description of sample locations

Appendix 1
Descriptions of samples from the Liaohe Group, which consists of five formations (from lower to upper): Langzishan Fm., Lieryu Fm., Gaojiayu Fm., Dashiqiao Fm. and Gaixian Fm

Sample number	Rock types	Location	Stratigraphic unit
LH05-011-1	deformed amphibolite	river bank south of Sankeli, Xiaonuzhai Town	Lieryu Fm., North Liaohe Group
LH05-012-1	foliated muscovite amphibolite	1km west of southeastern bridge of Mafeng Town	Lieryu Fm., North Liaohe Group
LH05-012-2	anthophyllite-rich rock	2km west of southeastern bridge of Mafeng Town	Lieryu Fm., North Liaohe Group
LH05-014-7	amphibolite	quarry of Huaziyu deposit	third member of Dashiqiao Fm., North Liaohe Group
LH05-016-1	metagabbro	Wangjiakan Reservior	Gaojiayu Fm., North Liaohe Group
LH05-026-1	amphibolite	Erdaogangzi of Maojiadian Town, Kuangdian County	Lieryu Fm., South Liaohe Group
LH05-034-1	coarse-grained hornblendite	roadside 2km east of Lianshanguan	upper Langzishan Fm., North Liaohe Group
LH05-035-4	fine-grained hornblendite	5km south of Shuiquan Town, Liaoyang City	first member of Dashiqiao Fm., North Liaohe Group
LH05-037-5	medium-grained hornblentite	roadside between Helan Town and Puzi River, Liaoyang	first member of Dashiqiao Fm., North Liaohe Group
LH05-038-1	fine-grained amphibolite	bridge south of Zhongpu Village, Helan Town	first member of Dashiqiao Fm., North Liaohe Group
LH05-040-1	fine-grained deformed amphibolite	river channel of Puzi River	first member of Dashiqiao Fm., North Liaohe Group

A.2. XRF reference materials

Standard		**JB-2**[#]	**2SD**[#]	JB-2	JB-2	AVRG	RSD%	Diff%	**JB-3**[*]	JB-3	JB-3	AVRG	RSD%	Diff%
SiO_2	wt%	**53.14**	**0.18**	53.61	53.23	53.42	*0.4*	*0.5*	**51.04**	51.31	51.3	51.31	*0.0*	*0.5*
TiO_2	wt%	**1.167**	**0.009**	1.18	1.18	1.18	*0.0*	*1.1*	**1.45**	1.42	1.41	1.42	*0.4*	*2.4*
AL_2O_3	wt%	**14.62**	**0.1**	15.02	15	15.01	*0.1*	*2.7*	**16.89**	17.6	17.53	17.57	*0.2*	*4.0*
Fe_2O_3	wt%	**14.28**	**0.12**	14.4	14.41	14.41	*0.0*	*0.9*	**11.88**	12.08	12.04	12.06	*0.2*	*1.5*
MnO	wt%	**0.213**	**0.0028**	0.21	0.21	0.21	*0.0*	*1.4*	**0.16**	0.18	0.18	0.18	*0.0*	*12.5*
MgO	wt%	**4.43**	**0.35**	4.78	4.72	4.75	*0.6*	*7.2*	**5.2**	5.25	5.25	5.25	*0.0*	*1.0*
CaO	wt%	**9.852**	**0.082**	9.92	9.91	9.92	*0.1*	*0.6*	**9.86**	9.83	9.79	9.81	*0.2*	*0.5*
Na_2O	wt%	**2.054**	**0.03**	1.98	1.91	1.95	*1.8*	*5.3*	**2.82**	2.69	2.71	2.70	*0.4*	*4.3*
K_2O	wt%	**0.4224**	**0.0059**	0.42	0.42	0.42	*0.0*	*0.6*	**0.78**	0.77	0.77	0.77	*0.0*	*1.3*
P_2O_5	wt%	**0.0969**	**0.0023**	0.09	0.1	0.10	*5.3*	*2.0*	**0.29**	0.3	0.3	0.30	*0.0*	*3.4*
V	ppm	**572.4**	**8.3**	552	548	550	*0.4*	*3.9*	**383**	381	375	378	*0.8*	*1.3*
Zn	ppm	**110.4**	**2.6**	108	109	109	*0.5*	*1.7*	**106**	105	100	103	*2.4*	*3.3*
Ba	ppm	**218.1**	**2.7**	187	225	206	*9.2*	*5.5*	**251**	234	243	239	*1.9*	*5.0*
Sr	ppm	**178.2**	**1.5**	181	183	182	*0.5*	*2.1*	**395**	404	405	405	*0.1*	*2.4*
Zr	ppm	**48.25**	**0.88**	52	54	53	*1.9*	*9.8*	**98.3**	92	92	92	*0.0*	*6.4*
TOTAL		100.40		101.73	101.21	101.47			100.51	101.57	101.42	101.49		
Standard		**JA-2**[#]	**2SD**[#]	JA-2	JA-2	AVRG	RSD%	Diff%	**JR-1**[*]	JR-1	JR-1	AVRG	RSD%	Diff%
SiO_2	wt%	**56.39**	**0.23**	56.38	56.39	56.39	*0.0*	*0.0*	**75.41**	74.97	75.18	75.08	*0.1*	*0.4*
TiO_2	wt%	**0.6695**	**0.007**	0.67	0.67	0.67	*0.0*	*0.1*	**0.1**	0.11	0.11	0.11	*0.0*	*10.0*
AL_2O_3	wt%	**15.51**	**0.11**	15.58	15.55	15.57	*0.1*	*0.4*	**12.89**	12.89	12.91	12.90	*0.1*	*0.1*
Fe_2O_3	wt%	**6.289**	**0.042**	6.43	6.42	6.43	*0.1*	*2.2*	**0.96**	0.91	0.91	0.91	*0.0*	*5.2*
MnO	wt%	**0.1092**	**0.0021**	0.11	0.11	0.11	*0.0*	*0.7*	**0.1**	0.1	0.1	0.10	*0.0*	*0.0*
MgO	wt%	**7.841**	**0.091**	7.98	7.96	7.97	*0.1*	*1.6*	**0.09**	0.17	0.18	0.18	*2.9*	*94.4*
CaO	wt%	**6.259**	**0.056**	6.28	6.26	6.27	*0.2*	*0.2*	**0.63**	0.7	0.7	0.70	*0.0*	*11.1*
Na_2O	wt%	**3.072**	**0.047**	2.89	2.98	2.94	*1.5*	*4.5*	**4.1**	3.87	3.94	3.91	*0.9*	*4.8*
K_2O	wt%	**1.779**	**0.015**	1.75	1.76	1.76	*0.3*	*1.3*	**4.41**	4.45	4.46	4.46	*0.1*	*1.0*
P_2O_5	wt%	**0.1519**	**0.0031**	0.16	0.16	0.16	*0.0*	*5.3*	**0.02**	0.02	0.02	0.02	*0.0*	*0.0*
V	ppm	**119.7**	**2.4**	132	137	135	*1.9*	*12.4*		bdl	bdl			
Zn	ppm	**64.5**	**2.3**	62	61	62	*0.8*	*4.7*	**30**	28	27	28	*1.8*	*8.3*
Ba	ppm	**308.4**	**5.1**	299	296	298	*0.5*	*3.5*	**40**	45	38	42	*8.4*	*3.8*
Sr	ppm	**245.8**	**3**	243	242	243	*0.2*	*1.3*	**30**	30	32	31	*3.2*	*3.3*
Zr	ppm	**108.5**	**2.6**	97	99	98	*1.0*	*9.7*	**101**	95	98	97	*1.6*	*4.5*
TOTAL		98.22		98.38	98.41	98.40			98.76	98.24	98.55			

[*] Govindaraju K (1994) Compilation of working values and sample descriptions for 383 geostandards. Geostnd Newsl 18(Special Issue):1–158.
[#] Jochum KP, Weis U, Schwager B, Stoll B, Wilson SA, Haug GH, Andreae MO, Enzweiler J (2016) Reference Values Following ISO Guidelines for Frequently Requested Rock Reference Materials. Geostandards and Geoanalytical Research 40(3):333–350.

A.3. ICP-MS reference materials (a) and sample replicates (b)

Appendix3a		BIR-1	2SD	BIR-1	BHVO-2	2SD	BHVO-2	JGb-2	2SD	JGb-2	JGb-2	JGb-2	2SD	2SD
		GeoReM[1]	GeoReM[1]		GeoReM[1]	GeoReM[1]		GeoReM[2]	GeoReM[2]	Dup 1	Dup 2	Average	ppm	%
Li	ppm	**3.203**	0.069	3.45	**4.500**	0.085	4.43	**13.7**	3.3	16.6	16.2	16.4	0.5	3.1
Sc	ppm	**43.21**	0.59	47.1	**31.83**	0.34	31.8	**24.0**	2.1	23.0	23.3	23.2	0.4	1.7
V	ppm	**320.6**	2.9	321	**318.2**	2.3	314	**175**	1	163	167	165	6	3.6
Cr	ppm	**392.9**	3.9	401	**287.2**	3.1	290	**126**	6	120	122	121	3	2.5
Co	ppm	**52.22**	0.57	53.5	**44.89**	0.32	44.8	**29.3**	4.9	24.5	25.1	24.8	0.7	2.9
Ni	ppm	**168.9**	1.9	171	**119.8**	1.2	118	**13.4**	0.9	13.4	13.5	13.5	0.1	0.6
Cu	ppm	**120.7**	1.6	124	**129.3**	1.4	129	**11.2**	0.6	10.4	10.6	10.5	0.3	3.2
Zn	ppm	**70.4**	1.1	71.8	**104**	1	104	**48.3**	0.7	49.6	46.9	48.3	4	7.8
Ga	ppm	**15.46**	0.23	16.5	**21.4**	0.2	21.6	**15.9**	0.00	16.0	16.2	16.1	0.2	1.2
Rb	ppm	**0.21**	0.0081	0.222	**9.261**	0.096	9.24	**2.10**	0.78	2.28	2.30	2.29	0.021	0.9
Sr	ppm	**108.6**	0.7	108	**394.1**	1.7	370	**440**	10	413	410	412	5	1.3
Y	ppm	**15.6**	0.17	16.2	**25.91**	0.28	25.5	**4.05**	1.20	3.53	3.53	3.53	0.00	0.1
Zr	ppm	**14.8**	0.22	15.9	**171.2**	1.3	174	**9.91**	3.48	9.26	7.93	8.60	1.88	21.9
Nb	ppm	**0.553**	0.014	0.573	**18.10**	0.2	18.3	**1.31**	0.92	0.678	0.692	0.685	0.019	2.7
Mo	ppm	**0.068**	0.021	0.072	**4.07**	0.16	4.48	**0.558**	0.234	0.450	0.350	0.400	0.141	35.2
Cs	ppm	**0.00646**	0.00072	0.006	**0.0996**	0.0022	0.099	**0.482**	0.137	0.580	0.579	0.580	0.002	0.3
Ba	ppm	**6.75**	0.13	7.23	**131**	1	131	**35.5**	2.50	35.8	35.8	35.8	0.0	0.0

(*continued*)

Appendix3a		BIR-1	2SD	BIR-1	BHVO-2	2SD	BHVO-2	JGb-2	2SD	JGb-2	JGb-2	JGb-2	2SD	2SD
La	ppm	**0.627**	0.012	0.629	**15.20**	0.08	15.0	**1.43**	0.25	1.52	1.48	1.50	0.05	3.4
Ce	ppm	**1.92**	0.023	1.96	**37.53**	0.19	36.8	**2.87**	0.73	3.14	3.14	3.14	0.01	0.2
Pr	ppm	**0.3723**	0.0047	0.386	**5.339**	0.028	5.26	**0.390**	0.069	0.414	0.410	0.412	0.006	1.6
Nd	ppm	**2.397**	0.043	2.52	**24.27**	0.25	24.5	**1.80**	0.22	1.93	1.92	1.93	0.01	0.7
Sm	ppm	**1.113**	0.018	1.17	**6.023**	0.057	6.11	**0.478**	0.085	0.535	0.531	0.533	0.006	1.2
Eu	ppm	**0.5201**	0.0047	0.553	**2.043**	0.012	2.08	**0.546**	0.107	0.627	0.623	0.625	0.006	1.0
Gd	ppm	**1.809**	0.021	1.90	**6.207**	0.038	6.13	**0.512**	0.138	0.604	0.607	0.606	0.005	0.8
Tb	ppm	**0.3623**	0.005	0.375	**0.939**	0.006	0.931	**0.098**	0.041	0.102	0.103	0.103	0.002	1.6
Dy	ppm	**2.544**	0.028	2.73	**5.280**	0.028	5.34	**0.605**	0.078	0.675	0.672	0.673	0.004	0.6
Ho	ppm	**0.5718**	0.0047	0.599	**0.9887**	0.0053	0.972	**0.128**	0.019	0.140	0.139	0.140	0.002	1.1
Er	ppm	**1.68**	0.015	1.72	**2.511**	0.014	2.44	**0.357**	0.048	0.389	0.391	0.390	0.003	0.9
Tm	ppm	**0.2558**	0.004	0.258	**0.3349**	0.0031	0.324	**0.055**	0.013	0.061	0.061	0.061	0.000	0.5
Yb	ppm	**1.631**	0.015	1.72	**1.994**	0.027	1.96	**0.355**	0.073	0.405	0.407	0.406	0.003	0.9
Lu	ppm	**0.2484**	0.0032	0.267	**0.2754**	0.0024	0.283	**0.055**	0.011	0.065	0.064	0.065	0.001	1.2
Hf	ppm	**0.5822**	0.0088	0.581	**4.470**	0.025	4.16	**0.261**	0.078	0.246	0.236	0.241	0.014	5.9
Ta	ppm	**0.0414**	0.002	0.040	**1.154**	0.019	1.05	**0.956**	1.538	0.052	0.050	0.051	0.003	5.5
Tl	ppm	**0.0021**	0.0007	0.004	**0.0224**	0.0015	0.023	**0.030**	0.00	0.018	0.019	0.018	0.001	4.5
Pb	ppm	**3.037**	0.049	3.21	**1.653**	0.038	1.57	**1.78**	1.59	0.933	0.917	0.925	0.023	2.5
Th	ppm	**0.0328**	0.0015	0.033	**1.224**	0.016	1.15	**0.151**	0.095	0.150	0.150	0.150	0.000	0.2
U	ppm	**0.01051**	0.00041	0.014	**0.412**	0.035	0.403	**0.035**	0.022	0.030	0.030	0.030	0.000	0.1

GeoReM[1] Jochum KP, Weis U, Schwager B, Stoll B, Wilson SA, Haug GH, Andreae MO, Enzweiler J (2016) Reference Values Following ISO Guidelines for Frequently Requested Rock Reference Materials. Geostandards and Geoanalytical Research 40(3):333–350.
GeoReM[2] average of published data 090619.

Appendix 3b

Appendix 3b		34–1 Dup 1	34–1 Dup 2	34–1 Average	2SD ppm	2SD %
Li	ppm	11.8	11.8	11.8	0.02	0.2
Sc	ppm	41.3	37.8	39.6	5.0	12.7
V	ppm	774	724	749	71	9.4
Cr	ppm	16.3	15.1	15.7	1.7	11.1
Co	ppm	60.5	58.1	59.3	3.4	5.8
Ni	ppm	19.8	18.9	19.3	1.3	6.5
Cu	ppm	36.5	37.0	36.7	0.7	1.9
Zn	ppm	141	140	141	2	1.7
Ga	ppm	24.0	23.5	23.8	0.7	2.8
Rb	ppm	36.0	35.5	35.8	0.7	2.1
Sr	ppm	177	174	176	5	2.8
Y	ppm	30.1	29.9	30.0	0.4	1.3
Zr	ppm	104	102	103	2	2.0
Nb	ppm	7.30	7.14	7.22	0.21	3.0
Mo	ppm	0.469	0.485	0.477	0.022	4.6
Cs	ppm	0.756	0.748	0.752	0.011	1.4
Ba	ppm	372	370	371	3	0.7
La	ppm	9.50	9.46	9.48	0.07	0.7
Ce	ppm	22.8	22.6	22.7	0.3	1.4
Pr	ppm	3.25	3.24	3.24	0.01	0.3
Nd	ppm	15.3	15.3	15.3	0.1	0.4
Sm	ppm	4.27	4.23	4.25	0.06	1.4
Eu	ppm	1.60	1.60	1.60	0.00	0.2
Gd	ppm	5.01	4.96	4.99	0.07	1.4
Tb	ppm	0.855	0.848	0.851	0.010	1.2
Dy	ppm	5.52	5.50	5.51	0.03	0.5
Ho	ppm	1.13	1.12	1.13	0.02	2.0
Er	ppm	3.12	3.07	3.09	0.06	2.1
Tm	ppm	0.454	0.450	0.452	0.006	1.4
Yb	ppm	2.98	2.97	2.97	0.02	0.7
Lu	ppm	0.457	0.452	0.454	0.007	1.6
Hf	ppm	2.80	2.76	2.78	0.06	2.0
Ta	ppm	0.429	0.425	0.427	0.004	1.0
Tl	ppm	0.167	0.164	0.166	0.004	2.2
Pb	ppm	2.53	2.54	2.53	0.01	0.4
Th	ppm	1.60	1.53	1.57	0.09	5.8
U	ppm	0.416	0.397	0.407	0.026	6.5

A.4. A) ^{238}U—^{206}Pb, B) ^{235}U—^{207}Pb and C) ^{232}Th—^{208}Pb errorchrons

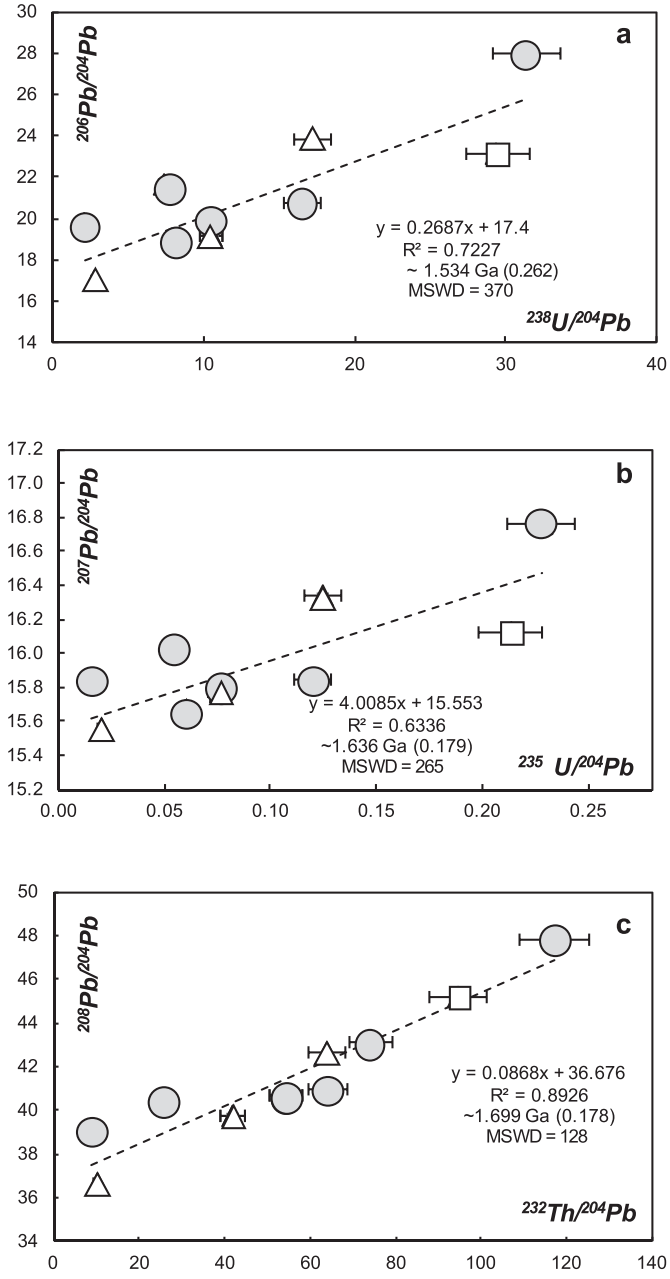

References

An, Y.H., 1990. A new division of the metamorphosed strata in the Jiaodong region: an account on the newly delimited Jiaodong Group and Jingshan Group. Shandong Geology 6, 97–103 (in Chinese with English abstract).

Bai, J., 1993. The Precambrian Geology and Pb-Zn Mineralization in the Northern Margin of North China Plateform. Geological Publishing House, Beijing, pp. 47–89 (in Chinese with English abstract).

Bai, J., Dai, F.Y., 1998. Archean crust of China. In: Ma, X., Bai, J. (Eds.), Precambrian Crust Evolution of China. Springer, Geological Publishing House, Beijing, pp. 15–86.

Blichert-Toft, J., Puchtel, I.S., 2010. Depleted mantle sources through time: evidence from Lu–Hf and Sm–Nd isotope systematics of Archean komatiites. Earth Planet. Sci. Lett. 297, 598–606.

Blichert-Toft, J., Chauvel, C., Albarede, F., 1997. Separation of Hf and Lu for high-precision isotope analysis of rock samples by magnetic sector-multiple collector ICP-MS. Contrib. Mineral. Petrol. 127, 248–260.

Braun, J., van der Beek, P., Batt, G., 2006. Quantitative Thermochronology: Numerical Methods for the Interpretation of Thermochronological Data. Cambridge University Press, Cambridge, pp. 24–27.

Cai, J.H., Yan, G.H., Mu, B.L., Xu, B.L., Shao, H.X., Xu, R.H., 2002. U-Pb and Sm-Nd isotopic ages of an alkaline syenite complex body in Liangtun-Kuangdongguo, Gai County, Liaoning Province, China and their geological significance. Acta Petrol. Sin. 18, 349–354.

Cao, G.Q., 1996. Early Precambrian Geology of Western Shandong. Geological Publishing House, Beijing, pp. 1–189 (in Chinese with English abstract).

Chauvel, C., Dupré, B., Jenner, G.A., 1985. The Sm-Nd age of Kambalda volcanics is 500 Ma too old! Earth Planet. Sci. Lett. 74 (4), 315–324.

Chen, S.L., Huan, Y.Q., Bing, Z.B., 2001. Characteristics of Palaeoproterozoic intrusive rocks and continental dynamic evolution of tectono-magmatism in the eastern Liaoning. Liaoning Geology 18, 43–50 (in Chinese with English abstract).

DePaolo, D.J., 1981. Trace element and isotopic effects of combined wall rock assimilation and fractional crystallization. Earth Planet. Sci. Lett. 53, 189–202.

Dong, C.Y., Wan, Y.S., Xie, H.Q., Nutman, A.P., Xie, S.W., Liu, S.J., Ma, M.Z., Liu, D.Y., 2017. The Mesoarchean Tiejiashan-Gongchangling potassic granite in the Anshan-Benxi area, North China Craton: origin by recycling of Paleo- to Eoarchean crust from U-Pb-Nd-Hf-O isotopic studies. Lithos 290-291, 116–135.

Dong, Y., Bi, J.H., Xing, D.H., Ge, W.C., Yang, H., Hao, Y.J., Zheng, J., Jing, Y., 2019. Geochronology and geochemistry of Liaohe Group and Liaoji granitoid in the Jiao-Liao-Ji Belt,

North China Craton: Implications for petrogenesis and tectonic evolution. Precambrian Res. 332, 105399.
Duggen, S., Portnyagin, M., Baker, J., Ulfbeck, D., Hoernle, K., Garbe-Schönberg, D., Grassineau, N., 2007. Drastic shift in lava geochemistry in the volcanic-front to rear-arc region of the Southern Kamchatkan subduction zone: Evidence for the transition from slab surface dehydration to sediment melting. Geochimica et Cosmochimica Acta 71, 452–480. https://doi.org/10.1016/j.gca.2006.09.018.
Faure, M., Lin, W., Monie, P., Bruguier, O., 2004. Palaeoproterozoic arc magmatism and collision in Liaodong Peninsula (north-east China). Terra Nova 16 (2), 75–80.
Garbe-Schönberg, C.-D., 1993. Simultaneous determination of thirty-seven trace elements in twenty-eight international rock standards by ICP-MS. Geostand. Newslett. 17 (1), 81–97.
Govindaraju, K., 1994. Compilation of working values and sample descriptions for 383 geostandards. Geostand. Newslett. 18, 1–158.
Guan, H., Sun, M., Simon, A.W., Zhou, X.H., Zhai, M.G., 2002. SHRIMP U-Pb zircon geochronology of the Fuping Complex: implications for formation and assembly of the North China Craton. Precambrian Res. 113, 1–18.
Guo, J.H., O'Brien, P.J., Zhai, M., 2002. High-pressure granulites in the Sanggan area, North China craton: metamorphic evolution, P-T paths and geotectonic significance. J. Metamorph. Geol. 20 (8), 741–756.
Guo, J.H., Sun, M., Zhai, M.G., 2005. Sm–Nd and SHRIMP U–Pb zircon geochronology of high-pressure granulites in the Sanggan area, North China Craton: timing of Paleoproterozoic continental collision. J. Asian Earth Sci. 24, 629–642.
Hao, D.F., Li, S.Z., Zhao, G.C., Sun, M., Han, Z.Z., Zhao, G.T., 2004. Origin and its constraint to tectonic evolution of Palaeoproterozoic granitoids in the eastern Liaoning and Jilin Province, North China. Acta Petrol. Sin. 20, 1409–1416 (in Chinese with English abstract).
Hastie, A.R., Kerr, A.C., Pearce, J.A., Mitchell, S.F., 2007. Classification of altered volcanic island arc rocks using immobile trace elements: development of the Th-Co discrimination diagram. J. Petrol. 48, 2341–2357.
Hawkesworth, C.J., Dhuime, B., Pietranik, A.B., Cawood, P.A., Kemp, A.I.S., Storey, C.D., 2010. The generation and evolution of the continental crust. J. Geol. Soc. 167, 229–248.
He, G.P., Ye, H.W., 1998. Two types of early Proterozoic metamorphism in the eastern Liaoning to southern Jilin and their tectonic implication. Acta Petrol. Sin. 14, 152–162 (in Chinese with English Abstract).
Heydoloph, K, Hoernle, K, Hauff, F, van den Bogaard, P, Portnyagin, M, Bindeman, I, Garbe-Schönberg, D, 2012. Along and across arc geochemical variations in NW Central America: Evidence for involvement of lithospheric pyroxenite. Geochimica et Cosmochimica Acta 84, 459–491. https://doi.org/10.1016/j.gca.2012.01.035.
Hofmann, A.W., 1988. Chemical differentiation of the Earth: the relationship between mantle, continental crust, and oceanic crust. Earth Planet. Sci. Lett. 90, 297–314.
Hu, G.W., 1992. The basic structural characteristics of the early Proterozoic Liaohe Group. Bulletin of Tianjin Institute of Geological Mineral Resources 26 (27), 179–188 (in Chinese with English Abstract).
Jacques G, Hoernle K, Gill J, Hauff F, Wehrmann H, Garbe-Schönberg D, van den Bogaard P, Bindeman I, Lara LE (2013) Across-arc geochemical variations in the Southern Volcanic Zone, Chile (34.5-38.0°S): constraints on mantle wedge and slab input compositions. Geochim. Cosmochim. Acta 123(0):218–243.
Jahn, B.M., Liu, D.Y., Wan, Y.S., Song, B., Wu, J.S., 2008. Archean crustal evolution of the Jiaodong Peninsula, China, as revealed by zircon SHRIMP geochronology, elemental and Nd-isotope geochemistry. Am. J. Sci. 308, 232–269.
Jiang, C.C., 1987. Precambrian Geology of Eastern Part of Liaoning and Jilin. Liaoning Science and Technology Press, Shenyang, pp. 1–299 (in Chinese with English abstract).
Jochum, K.P., Weis, U., Schwager, B., Stoll, B., Wilson, S.A., Haug, G.H., Andreae, M.O., Enzweiler, J., 2016. Reference values following ISO guidelines for frequently requested rock reference materials. Geostand. Geoanal. Res. 40, 333–350.
Khanna, T.C., Bizimis, M., Yogodzinski, G.M., Mallic, S., 2014. Hafnium–neodymium isotope systematics of the 2.7 Ga Gadwal greenstone terrane, Eastern Dharwar craton, India: Implications for the evolution of the Archean depleted mantle. Geochim. Cosmochim. Acta 127, 10–24.
Kim, C.B., Turek, A., Chang, H.W., Park, Y.S., Ahn, K.S., 1999. U-Pb zircon ages for Precambrian and Mesozoic plutonic rocks in the Seoul-Cheongju-Chooncheon area. Gyeonggi massif, Korea, Geochemical Journal 33, 379–397.
Kim, J., Cho, M., 2003. Low-pressure metamorphism and leucogranite magmatism, northeastern Yeongnam Massif. Korea: Implication for Paleopreoterozoic crustal evolution, Precambrian Research 122, 235–251.
Kim, S.R., Jon, G.P., 1996. Archean strata in North Korea, in: Institute of Geology, State Academy of Sciences, DPR of Korea (Ed.), Geology of Korea, Foreign Language Book Publishing House, Pyeongyang, pp. 14–30.
Kröner, A., Cui, W.Y., Wang, S.Q., Wang, C.Q., Nemchin, A.A., 1998. Single zircon ages from high-grade rocks of the Jianping Complex, Liaoning Province, NE China. Journal of Asian Earth Science 16, 519–532.
Kröner, A., Wilde, S.A., Li, J.H., Wang, K.Y., 2005. Age and evolution of a late Archaean to early Palaeozoic upper to lower crustal section in the Wutaishan/Hengshan/Fuping terrain of northern China. Journal of Asian Earth Science 24, 577–595.
Kröner, A., Wilde, S.A., Zhao, G.C., O'Brien, P.J., Sun, M., Liu, D.Y., Wan, Y.S., Liu, S.W., Guo, J.H., 2006. Zircon geochronology and metamorphic evolution of mafic dykes in the Hengshan Complex of northern China: evidence for late Palaeoproterozoic extension and subsequent high-pressure metamorphism in the North China Craton. Precambrian Res. 146, 45–67.
LBGMR (Liaoning Bureau of Geology and Mineral Resources), 1989. Regional Geology of Liaoning Province. Geological Publishing House, Beijing, pp. 1–526 (in Chinese with English abstract).
Lee, B.C., Oh, C.W., Cho, D.L., Yi, K., 2019. Paleoproterozoic (2.0–1.97 Ga) subduction-related magmatism on the north–central margin of the Yeongnam Massif, Korean Peninsula, and its tectonic implications for reconstruction of the Columbia supercontinent. Gondwana Res. 72, 34–53.
Lee, S.G., Shin, S.C., Jin, M.S., Ogasawara, M., Yang, M.K., 2005. Two Paleoproterozoic strongly peraluminous granitic plutons (Nonggeori and Naedeokri granites) at the northeastern part of Yeongnam Massif. Korea: Geochemical and isotopic constraints in East Asian crustal formation history, Precambrian Research 139, 101–120.
Li, S.Z., Yang, Z.S., 1997. Types and genesis of palaeoproterozoic granites in the Jiao-Liao Massif. Northwest Geology 43 (6), 21–27 (in Chinese with English abstract).
Li, S.Z., Zhao, G.C., 2007. SHRIMP U-Pb zircon geochronology of the Liaoji granitoids: constraints on the evolution of the Paleoproterozoic Jiao-Liao-Ji belt in the Eastern Block of the North China Craton. Precambrian Res. 158, 1–16.
Li, S.Z., Yang, Z.S., Liu, Y.J., 1996. Preliminary analysis on layered gravitational sliding structure of the Palaeoproterozoic orogenic belt in Liaodong Peninsula. Journal of Changchun University of Earth Science 26, 305–309 (in Chinese with English abstract).
Li, S.Z., Yang, Z.S., Liu, Y.J., Liu, J.L., 1997a. Emplacement model of Palaeoproterozoic early-granite in the Jiao-Liao-Ji Area and its relation to layered gravitaional sliding stucture. Acta Petrol. Sin. 13, 189–202 (in Chinese with English abstract).
Li, Y.G., Zhai, M.G., Liu, W.J., Guo, J.H., 1997b. Sm-Nd geochronology of the high-pressure basic granulite in Laixi, Eastern Shandong. Sci. Geol. Sin. 32 (3), 283–290 (in Chinese with English abstract).
Li, S.Z., Han, Z.Z., Liu, Y.J., Yang, Z.S., 2001a. Geological and geochemical constraints on Palaeoproterozoic pre-Orogenic deep processes in the Jiao-Liao Block. Sci. Geol. Sin. 36, 184–194 (in Chinese with English abstract).
Li, S.Z., Han, Z.Z., Liu, Y.J., Yang, Z.S., Ma, R., 2001b. Regional metamorphism of the Liaohe Group: implications for continental dynamics. Geological Review 47, 9–18 (in Chinese with English abstract).
Li, S.Z., Zhao, G.C., Sun, M., Hao, D.F., Luo, Y., Yang, Z.Z., 2003. Paleoproterozoic tectonothermal evolution and deep crustal processes of the Jiao-Liao Block. Acta Geol. Sin. 73, 328–340.
Li, S.Z., Zhao, G.C., Sun, M., Wu, F.Y., Liu, J.Z., Hao, D.F., Han, Z.Z., Luo, Y., 2004. Mesozoic not Paleoproterozoic SHRIMP U–Pb zircon ages of two Liaoji granites, Eastern Block, North China Craton. Int. Geol. Rev. 46, 162–176.
Li, S.Z., Zhao, G.C., Sun, M., Han, Z.Z., Hao, D.F., Luo, Y., Xia, X.P., 2005a. Deformation history of the Paleoproterozoic Liaohe assemblage in the Eastern Block of the North China Craton. J. Asian Earth Sci. 24, 659–674.
Li, S.Z., Zhao, G.C., Sun, M., Han, Z.Z., Zhao, G.T., 2005b. Nd isotopic characteristics of the South and North Liaohe Groups and tectonic implications. Geochimica Cosmochimica Acta 69, A863.
Li, S.Z., Zhao, G.C., Sun, M., Han, Z.Z., Zhao, G.T., Hao, D.F., 2006. Are the South and North Liaohe Groups different exotic terranes? Nd isotope constraints on the Jiao-Liao-Ji orogen. Gondwana Res. 9, 198–208.
Li, S.Z., Zhao, G.C., Wilde, S.A., Zhang, J., Sun, M., Zhang, G.W., Dai, L.M., 2010. Deformation history of the Hengshan–Wutai–Fuping Complexes: Implications for the evolution of the Trans-North China Orogen. Gondwana Res. 18, 611–631.
Li, S.Z., Zhao, G.C., Santosh, M., Liu, X., Dai, L.M., 2011a. Palaeoproterozoic tectono-thermal evolution and deep crustal processes in the Jiao-Liao-Ji Belt, North China craton: a review. Geol. J. 46, 525–543.
Li, X.P., Guo, J.H., Zhao, G.C., Li, H.K., Song, Z.J., 2011b. Formation of the Paleoproterozoic calc-silicate and high-pressure mafic granulite in the Jiaobei terrane, eastern Shandong, China. Acta Petrol. Sin. 27 (4), 961–968 (in Chinese with English abstract).
Li, S.Z., Zhao, G.C., Liu, X., Dai, L.M., Suo, Y.H., Song, M.C., Wang, P.C., 2012. Structural evolution of the southern segment of the Jiao-Liao-Ji Belt, North China Craton. Precambrian Res. 200–203, 59–73.
Li, S.Z., Suo, Y.H., Li, X.Y., Liu, B., Dai, L.M., Wang, G.Z., Zhou, J., Li, Y., Liu, Y.M., Cao, X.Z., Somerville, I., Mu, D.L., Zhao, S.J., Liu, J.P., Meng, F., Zhen, L.B., Zhao, L.T., Zhu, J.J., Yu, S.Y., Liu, Y.J., Zhang, G.W., 2018. Microplate tectonics: new insights from micro-blocks in the global oceans, continental margins and deep mantle. Earth Sci. Rev. 185, 1029–1064.
Li, S.Z., Li, X., Wang, G., Liu, Y., Wang, Z., Wang, T., Cao, X., Guo, X., Somerville, I., Li, Y., Zhou, J., Dai, L., Jiang, S., Zhao, H., Wang, Y., Wang, G., Yu, S., 2019. Global Meso-Neoproterozoic plate reconstruction and formation mechanism for Precambrian basins: Constraints from three cratons in China. Earth Sci. Rev. 198, 102946.
Li, T., Santosh, M., 2018. Neoarchean-Paleoproterozoic terrane assembly and Wilson cycle in the North China Craton: an overview from the central segment of the Trans-North China Orogen. Earth Sci. Rev. 182, 1–27.
Lin, W.W., Zhao, Y.M., Zhao, G.H., Xu, Y., Zhao, W.G., 1998. Structural of Jingshan Group and the study of gold. Shandong Geology 14 (4), 42–49 (in Chinese with English abstract).
Liu, C.H., Zhao, G.C., Liu, F.L., Cai, J., 2018b. The southwestern extension of the Jiao-Liao-Ji belt in the North China Craton: Geochronological and geochemical evidence from the Wuhe Group in the Bengbu area. Lithos 304–307, 258–279.
Liu, D.Y., Nutman, A.P., Compston, W., Wu, J.S., Shen, Q.H., 1992. Remnants of 3800 crust in the Chinese part of the Sino-Korean craton. Geology 20, 339–342.
Liu, F.L., Liu, P.H., Wang, F., Liu, C.H., Cai, J., 2015. Progresses and overviews of voluminous meta-sedimentary series within the Paleoproterozoic Jiao-Liao-Ji orogenic/mobile belt, North China Craton. Acta Petrol. Sin. 31, 2816–2846 (in Chinese with English abstract).
Liu, F.L., Liu, L.S., Liu, P.H., Wang, F., Cai, J., Liu, J.H., Wang, W., Ji, L., 2017a. A relic slice of Archean–early Paleoproterozoic basement of Jiaobei Terrane identified within the Sulu UHP belt: evidence from protolith and metamorphic ages from meta-mafic rocks, TTG–granitic gneisses, and metasedimentary rocks in the Haiyangsuo region. Precambrian Res. 303, 117–152.
Liu, F.L., Liu, C.H., Itano, K., Iizuka, T., Cai, J., Wang, F., 2017b. Geochemistry, U-Pb dating, and Lu-Hf isotopes of zircon and monazite of porphyritic granites within the Jiao-Liao-Ji orogenic belt: implications for petrogenesis and tectonic setting. Precambrian Res. 300, 78–106.

Liu, F.L., Liu, L.S., Cai, J., Liu, P.H., Wang, F., Liu, C.H., Liu, J.L., 2019b. A widespread Paleoproterozoic partial melting event within the Jiao-Liao-Ji Belt, North China Craton: Zircon U-Pb dating of granitic leucosomes within pelitic granulites and its tectonic implications. Precambrian Res. 326, 155–173.

Liu, J., Zhang, J., Liu, Z.H., Yin, C.Q., Zhao, C., Li, Z., Yang, Z.J., Dou, S.H., 2018a. Geochemical and geochronological study on the Paleoproterozoic rock assemblage of the Xiuyan region: new constraints on an integrated rift-and-collision tectonic process involving the evolution of the Jiao-Liao-Ji Belt, North China Craton. Precambrian Res. 310, 179–197.

Liu, J.H., Liu, F.L., Ding, Z.J., Liu, C.H., Yang, H., Liu, P.H., Wang, F., Meng, E., 2013a. The growth, reworking and metamorphism of early Precambrian crust in the Jiaobei terrane, the North China Craton: Constraints from U-Th-Pb and Lu-Hf isotopic systematics, and REE concentrations of zircon from Archean granitoid gneisses. Precambrian Res. 224, 287–303.

Liu, J.H., Liu, F.L., Ding, Z.J., Yang, H., Liu, C.H., Liu, P.H., Xiao, L.L., Zhao, L., Meng, E., Geng, J.Z., 2013b. U–Pb dating and Hf isotope study of detrital zircons from the Zhifu Group, Jiaobei Terrane, North China Craton: provenance and implications for Precambrian crustal growth and evolution. Precambrian Res. 235, 230–250.

Liu, P.H., Liu, F.L., Tian, Z.H., Cai, J., Ji, L., Wang, F., 2019a. Petrological and geochronological evidence for Paleoproterozoic granulite-facies metamorphism of the South Liaohe Group in the Jiao-Liao-Ji Belt, North China Craton. Precambrian Res. 327, 121–143.

Liu, S.W., Wang, M.J., Wan, Y.S., Guo, R.R., Wang, W., Wang, K., Guo, B.R., Fu, J.H., Hu, F.Y., 2017c. A reworked ~3.45 Ga continental microblock of the North China Craton: constraints from zircon U-Pb-Lu-Hf isotopic systemtatics of the Archean Beitai-Waitoushan migmatite-syenograntie complex. Precambrian Res. 303, 332–354.

Liu, W.J., Zhai, M.G., Li, Y.G., 1998. Metamorphism of the highpressure basic granulite in Laixi. Eastern Shandong, China: Acta Petrologica Sinica 14, 449–459 (in Chinese with English abstract).

Liu, Y.J., Li, S.Z., 1996. Palaeoproterozoic granite in the area from Haicheng City, via Dashiqiao City to Jidong Town. Liaoning Geology 1, 10–18 (in Chinese with English abstract).

Lu, L.Z., 1996. The Precambrian metamorphic geology and tectonic evolution of the Jiao-Liao massif. Journal of Changchun University of Earth Science 26, 25–32.

Lu, L.Z., Xu, X.C., Liu, F.L., 1996. Early Precambrian khondalites in North China: Changchun. Jilin Science and Technology Press, pp. 195–235 (in Chinese with English Abstract).

Lu, S.N., Zhao, G.C., Wang, H.C., Hao, G.J., 2008. Precambrian metamorphic basement and sedimentary cover of the North China Craton: a review. Precambrian Res. 160, 77–93.

Lu, X.P., Wu, F.Y., Lin, J.Q., Sun, D.Y., Zhang, Y.B., Guo, C.L., 2004a. Geochronological successions of the early Precambrian granitic magmatism in southern Liaoning Peninsula and its constraints on tectonic evolution of the North China Craton. Chinese Journal of Geology. 39, 123–139 (in Chinese with English abstract).

Lu, X.P., Wu, F.Y., Zhang, Y.B., Zhao, C.B., Guo, C.L., 2004b. Emplacement age and tectonic setting of the Paleoproterozoic Liaoji granites in Tonghua area, southern Jilin Province. Acta Petrol. Sin. 20, 381–392 (in Chinese with English abstract).

Lu, X.P., Wu, F.Y., Guo, J.H., Yin, C.J., 2005. Late Paleoproterozoic granitic magmatism and crustal evolution in Tonghua region, northeast China. Acta Petrol. Sin. 21, 721–736.

Lu, X.P., Wu, F.Y., Guo, J.H., Wilde, S.A., Yang, J.H., Liu, X.M., Zhang, X.O., 2006. Zircon U–Pb geochronological constraints on the Palaeoproterozoic crustal evolution of the Eastern block in the North China Craton. Precambrian Res. 146, 138–164.

Luo, Y., Sun, M., Zhao, G.C., Li, S.Z., Xu, P., Ye, K., Xia, X.P., 2004. LA-ICP-MS U-Pb zircon ages of the Liaohe Group in the Eastern Block of the North China Craton: constraints on the evolution of the Jiao-Liao-Ji Belt. Precambrian Res. 134, 349–371.

Luo, Y., Sun, M., Zhao, G.C., Li, S.Z., Ayers, J.C., Xia, X.P., Zhang, J.H., 2008. A comparison of U-Pb and Hf isotopic compositions of detrital zircons from the North and South Liaohe Groups: constraints on the evolution of the Jiao-Liao-Ji Belt, North China Craton. Precambrian Res. 163, 279–306.

Manikyamba, C., Khanna, T.C., 2007. Crustal growth processes as illustrated by the Neoarchaean intraoceanic magmatism from Gadwal greenstone belt, Eastern Dharwar Craton, Inida. Gondwana Res. 11, 476–491.

Meng, E., Liu, F.L., Liu, P.H., Liu, C.H., Yang, H., Wang, F., Shi, J.R., Cai, J., 2014. Petrogenesis and tectonic significance of Paleoproterozoic meta-mafic rocks from central Liaodong Peninsula, northeast China: evidence from zircon U–Pb dating and in situ Lu–Hf isotopes, and whole-rock geochemistry. Precambrian Res. 247, 92–109.

Naeraa, T., Schersten, A., Rosing, M.T., Kemp, A.I.S., Hoffmann, J.E., Kokfelt, T.F., Whitehouse, M.J., 2012. Hafnium isotope evidence for a transition in the dynamics of continental growth 3.2 Gyr ago. Nature 485, 627–630.

Nebel, O., Capitanio, F.A., Moyen, J.-F., Weinberg, R.F., Clos, F., Nebel-Jacobsen, Y.J., Cawood, P.A., 2018. When crust comes of age: on the chemical evolution of Archaean, felsic continental crust by crustal drip tectonics. Phil. Trans. R. Soc. A 376, 20180103.

Oh, C.W., Lee, B.C., Yi, S.-B., Ryu, H.I., 2019. Correlation of Paleoproterozoic igneous and metamorphic events of the Korean Peninsula and China; its implication to the tectonics of Northeast Asia. Precambrian Res. 326, 344–362.

Paek, R.J., Jon, G.P., 1996. Lower Proterozoic era in North Korea, in: Institute of Geology, State Academy of Sciences, DPR of Korea (Ed.), Geology of Korea., Foreign Language Book Publishing House, Pyeongyang, pp. 31–51.

Pearce, J.A., 1982. Trace element characteristics of lavas from destructive plate boundaries, in: Thorpe, R.S. (Ed.), Andesites. John Wiley & Sons, pp. 525-548.

Pearce, J.A., 1996. Sources and settings of granitic rocks. Episodes 19, 120–125.

Pearce, J.A., 2008. Geochemical fingerprinting of oceanic basalts with applications to ophiolite classification and the search for Archean oceanic crust. Lithos 100, 14–48.

Peng, Q.M., Palmer, M.R., 1995. The Palaeoproterozoic boron deposits in eastern Liaoning, China-a metamorphosed evaporite. Precambrian Res. 72 (3–4), 185–197.

Peng, Q.M., Palmer, M.R., Lu, J.W., 1998. Geology and geochemistry of the Paleoproterozoic borate deposits in Liaoning-Jilin, northeastern China: evidence of meta-evaporites. Hydrobiologia 381, 51–57.

Portnyagin, M, Bindeman, I, Hoernle, K, Hauff, F, 2007. Geochemistry of primitive lavas of the Central Kamchatka Depression: Magma Generation at the Edge of the Pacific Plate. In: Volcanism and Subduction: The Kamchatka Region; Eichelberger J, Gordeev E, Kasahara M, Izbekov P, Lees J (eds). Geophysical Monograph Series, American Geophysical Union, Washington D.C., USA 172, 199–239.

Sadofsky, S., Hoernle, K., Duggen, S., Hauff, F., Werner, R., Garbe-Schönberg, D., 2009. Geochemical variations in the Cocos Plate subducting beneath Central America: implications for the composition of arc volcanism and the extent of the Galápagos Hotspot influence on the Cocos oceanic crust. Int. J. Earth Sci. 98, 901–913.

Santosh, M., 2010. Assembling North China Craton within the Columbia supercontinent: the role of double-sided subduction. Precambrian Res. 178, 149–167.

Santosh, M., Wilde, S.A., Li, J.H., 2007. Timing of Paleoproterozoic ultrahigh-temperature metamorphism in the North China Craton: evidence from SHRIMP U–Pb zircon geochronology. Precambrian Res. 159, 178–196.

Santosh, M., Liu, D.Y., Shi, Y.R., Liu, S.J., 2013. Paleoproterozoic accretionary orogenesis in the North China Craton: a SHRIMP zircon study. Precambrian Res. 227, 29–54.

Santosh, M., Yang, Q.Y., Teng, X.M., Li, T., 2015. Paleoproterozoic crustal growth in the North China Craton: evidence from the Lüliang Complex. Precambrian Res. 263, 197–231.

Schaefer, B.F., 1998. Insights into Proterozoic tectonics from the southern Eyre Peninsula, South Australia. Adel University PhD Thesis. (Unpubl).

Schaefer, B.F., 2016. Radiogenic Isotope Geochemistry: A Guide for Industry Professionals. Camb University Press. 212pp.

SD4IGMR (Shandong No. 4 Institute of Geological and Mineral Resources), 2005. Regional Geology of Shandong Province. Shandong Map Publishing House, Beijing, pp. 1–964 (in Chinese with English abstract).

Shen, Y.Z., Hu, A.Q., 1986. K-Ar age contour map of Liaohe Group, Central Liaoning, and its geological implications. Geochimica 1, 36–41 (in Chinese with English abstract).

Song, B., Nutman, A.P., Liu, D.Y., Wu, J.S., 1996. The Oldest Rock on Earth 3800 to 2500 Ma crustal evolution in the Anshan area of Liaoning Province, northeastern China. Precambrian Res. 78 (1–3), 79–94.

Sun, M., Armstrong, R.L., Lambert, R.S., Jiang, C.C., Wu, J.H., 1993. Petrochemistry and Sr, Pb and Nd isotopic geochemistry of Palaeoproterozoic Kuandian Complex, the eastern Liaoning Province, China. Precambrian Res. 62, 171–190.

Sun, M., Zhang, L.F., Wu, J.H., 1996. The origin of the Early Proterozoic Kuandian Complex: evidence from geochemistry. Acta Geol. Sin. 70, 207–222 (in Chinese with English abstract).

Sun, S.-s., McDonough, W.F., 1989. Chemical and isotopic systematics of oceanic basalts: implications for mantle composition and processes. In: Saunders, A.D., Norry, M.J. (Eds.), Magmatism in the Ocean Basins. Blackwell, London, pp. 313–345.

Tam, P.K., Zhao, G.C., Liu, F.L., Zhou, X.W., Sun, S., Li, S.Z., 2011. Timing of metamorphism in the Paleoproterozoic Jiao-Liao-Ji Belt: New SHRIMP U–Pb zircon dating of granulites, gneisses and marbles of the Jiaobei massif in the North China Craton. Gondwana Res. 19, 150–162.

Tam, P.Y., Zhao, G.C., Liu, F.L., Zhou, X.W., Sun, M., Li, S.Z., 2012a. SHRIMP U–Pb zircon ages of high-pressure mafic and pelitic granulites and associated rocks in the Jiaobei massif: constraints on the metamorphic ages of the Paleoproterozoic Jiao-Liao-Ji Belt in the North China Craton. Gondwana Res. 19, 150–162.

Tam, P.Y., Zhao, G., Zhou, X., Sun, M., Guo, J., Li, S., Yin, C., Wu, M., He, Y., 2012b. Metamorphic P-T path and implications of high-pressure pelitic granulites from the Jiaobei massif in the Jiao-Liao-Ji Belt, North China Craton. Gondwana Res. 22, 104–117.

Tam, P.Y., Zhao, G., Sun, M., Li, S., Wu, M., Yin, C., 2012c. Petrology and metamorphic P-T path of high-pressure mafic granulites from the Jiaobei massif in the Jiao-Liao-Ji Belt, North China Craton. Lithos 155, 94–109.

Tang, J., Zheng, Y.F., Wu, Y.B., Gong, B., Liu, X.M., 2007. Geochronology and geochemistry of metamorphic rocks in the Jiaobei terrane: constraints on its tectonic affinity in the Sulu orogen. Precambrian Res. 152, 48–82.

Theriault, R.J., Ross, G.M., 1991. Nd isotopic evidence for crustal recycling in the ca. 2.0 Ga subsurface of western Canada. Canadian Journal of Earth Science 28, 1140–1147.

Todt, W., Cliff, R.A., Hanser, A., Hofmann, A.W., 1996. Evaluation of a 202Pb-205Pb double spike for high precision lead isotope analyses. In: Basu, A., Hart, S. (Eds.), Earth Processes: Reading the Isotopic Code, Geophysical Monograph 95. AGU, Washington, pp. 429–437.

Wan, Y.S., Liu, D.Y., Song, B., Wu, J.S., Yang, C.H., Zhang, Z.Q., Geng, Y.S., 2005. Geochemical and Nd isotopic compositions of 3.8 Ga meta-quartz dioritic and trondhjemitic rocks from the Anshan area and their geological significance. J. Asian Earth Sci. 24, 563–575.

Wan, Y.S., Song, B., Liu, D.Y., Wilde, S.A., Wu, J.S., Shi, Y.R., Yin, X.Y., Zhou, H.Y., 2006. SHRIMP U-Pb zircon geochronology of Paleoproterozoic metasedimentary rocks in the North China Craton: evidence for a major Late Paleoproterozoic tectonothermal event. Precambrian Res. 149, 249–271.

Wan, Y.S., Liu, D.Y., Dong, C.Y., Liu, S.J., Wang, S.J., Yang, E.X., 2011. The impact of high-grade metamorphism on the U-Th-Pb system of zircons: a case study of zircon dating of meta-diorite in Qixia area, eastern Shandong. Earth Science Frontiers 18 (2), 17–25 (in Chinese with English abstract).

Wan, Y.S., Liu, D.Y., Nutman, A., Zhou, H.Y., Dong, C.Y., Yin, X.Y., Ma, M.Z., 2012. Multiple 3.8–3.1 Ga tectono-magmatic events in a newly discovered area of ancient rocks (the Shengousi Complex), Anshan, North China Craton. J. Asian Earth Sci. 54–55, 18–30.

Wang, C.W., Liu, Y.J., Li, D.T., 1997. New evidences on the correlation of Liaohe Lithogroup between the southern and the northern regions in eastern Liaoning Province. Journal of Changchun University of Science and Technology 1, 17–24 (in Chinese with English abstract).

Wang, L.M., Yan, Y.M., 1992. The archaean tonalites in Qixia area, Shandong. Shandong Geology 8 (1), 80–87 (in Chinese with English abstract).

Wang, M.J., Liu, S.W., Fu, J.H., Wang, K., Guo, R.R., Guo, B.R., 2017. Neoarchean TTG gneisses in southern Liaoning Province and their constraints on crustal growth and the nature of the Liao-Ji Belt in the Eastern Block. Precambrian Res. 303, 183–207.
Wang, W., Yang, E.X., Zhai, M.G., Wang, S.J, Santosh, M., Du, L.L. Xie, H.Q., Lv, B., Wan, Y.H. 2013. Geochemistry of ~2.7 Ga basalts from Taishan area: Constraints on the evolution of early Neoarchean granite-greenstone belt in western Shandong Province, China. Precambrian Res. 224, 94–109.
Wu, M.L., Zhao, G.C., Sun, M., Li, S.Z., He, Y.H., Bao, Z.A., 2013. Zircon U-Pb geochronology and Hf isotopes of major lithologies from the Yishui Terrane: Implications for the crustal evolution of the Eastern Block, North China Craton. Lithos 170–171, 164–178.
Wu, M.L., Zhao, G.C., Sun, M., Li, S.Z., Bao, Z.A., Tam, P.K., Eizenhöefer, P.R., He, Y.H., 2014. Zircon U-Pb geochronology and Hf isotopes of major lithologies from the Jiaodong Terrane: implications for the crustal evolution of the Eastern Block of the North China Craton. Lithos 190-191, 71–84.
Xia, X.P., Sun, M., Zhao, G.C., Luo, Y., 2006. LA–ICP-MS U–Pb geochronology of detrital zircons from the Jining Complex, North China Craton and its tectonic significance. Precambrian Res. 144, 199–212.
Xie, L.W., Yang, J.H., Wu, F.Y., Yang, Y.H., Wilde, S.A., 2011. PbSL dating of garnet and staurolite: Constraints on the Paleoproterozoic crustal evolution of the Eastern Block, North China Craton. J. Asian Earth Sci. 42, 142–154.
Xu, B.L., Yan, G.H., Mo, B.L., 1998. Rb-Sr age and its implication of Alkaline from Liangtun to Kuangdonggou, Gaixian City, Liaoning. Chin. Sci. Bull. 43, 1885–1887 (in Chinese).
Xu, W., Liu, F.L., 2019. Geochronological and geochemical insights into the tectonic evolution of the Paleoproterozoic Jiao-Liao-Ji Belt, Sino-Korean Craton. Earth Sci. Rev. 193, 162–198.
Xu, W., Liu, F.L., Tian, Z.H., Liu, L.S., Ji, L., Dong, Y.S., 2018a. Source and petrogenesis of Paleoproterzoic meta-mafic rocks intruding into the North Liaohe Group: Implications for back-arc etension prior to the formation of the Jiao-Liao-Ji Belt, North China Craton. Precambrian Res. 307, 66–81.
Xu, W., Liu, F.L., Santosh, M., Liu, P.H., Tian, Z.H., Dong, Y.S., 2018b. Constraints of mafic rocks on a Paleoproterozic back-arc in the Jiao-Liao-Ji Belt. North China Craton. J. Asian Earth Sci. 166, 195–209.
Xu, W., Liu, F.L., Wang, F., Santosh, M., Dong, Y.S., 2020. Palaeoproterozoic tectonic evolution of the Jiao–Liao–Ji Belt, North China Craton: geochemical and isotopic evidence from ca. 2.17 Ga felsic tuff. Geol. J. 55, 409–424.
Yang, Z.S., Li, S.G., Yu, B.X., Gao, D.H., Gao, C.G., 1988. Structural deformation and mineralization in the Early Proterozoic Liaojitite suite, eastern Liaoning province, China. Precambrian Res. 39, 31–38.
Yu, Z.C., 1996. New progress of research on the Fenzishan Group in the Pingdu- Laizhou area in the west of Jiaobei region. Shandong Geology 12 (1), 24–34.
Zhai, M.G., 2011. Cratonization and formation of the North China Craton. Science in China (Series D) 41 (8), 1037–1046.
Zhai, M.G., Liu, W.J., 2003. Palaeoproterozoic tectonic history of the North China craton: a review. Precambrian Res. 122, 183–199.
Zhai, M.G., Santosh, M., 2011. The Early Precambrian odyssey of the North China Craton: a synoptic overview. Gondwana Res. 20, 6–25.
Zhai, M.G., Guo, J.H., Yan, Y.H., Li, Y.G., Han, X.L., 1993. Discovery of high-pressure basic granulite terrain in the North China Archean Craton and preliminary-study. Science in China (Series B) 36, 1402–1408 (in Chinese with English abstract).
Zhai, M.G., Cong, B.L., Guo, J.H., Liu, W.J., Li, Y.G., Wang, Q.C., 2000. Sm–Nd geochronology and petrography of garnet pyroxene granulites in the northern Sulu region of China and their geotectonic implication. Lithos 52, 23–33.
Zhai, M.G., Ni, Z.Y., Oh, C.W., Guo, J.H., Cho, S.G., 2005. SHRIMP zircon age of a Proterozoic rapakivi granite batholith in the Gyeonggi massif (South Korea) and its geological implications. Geol. Mag. 142, 23–30.
Zhang, J., Zhao, G.C., Sun, M., Wilde, S.A., Li, S.Z., Liu, S.W., 2006. High-pressure mafic granulites in the Trans-North China Orogen: tectonic significance and age. Gondwana Res. 9, 349–362.
Zhang, J., Zhao, G.C., Li, S.Z., Sun, M., Liu, S.W., Wilde, S.A., Kröner, A., Yin, C.Q., 2007. Deformation history of the Hengshan Complex: implications for the tectonic evolution of the Trans-North China Orogen. J. Struct. Geol. 29, 933–949.
Zhang, Q.S., Yang, Z.S., 1988. Early Crust and Mineral Deposits of Liaodong Peninsula, China. Geological Publishing House, Beijing, pp. 218–450 (in Chinese with English abstract).
Zhang, Q.S., Yang, Z.S., Liu, L.D., 1988. Early Crust and Mineral Deposits of the Liaodong Peninsula. Geological Publishing House, Beijing, China (in Chinese with English abstract).
Zhang, W., Liu, F.L., Cai, J., Liu, C.H., Liu, J.H., Liu, P.H., Liu, L.S., Wang, F., Yang, H., 2018. Geochemistry, zircon U-Pb dating and tectonic implications of the Palaeoproterozoic Ji'an and Laoling groups, northeastern Jiao-Liao-Ji Belt, North China Craton. Precambrian Res. 314, 264–287.
Zhang, X.O., Cawood, P., Wilde, S., Liu, R., Song, H., Li, W., Snee, L., 2003. Geology and timing of mineralization at the Cangshang gold deposit, north-western Jiaodong Peninsula, China. Mineral. Deposita 38, 141–153.
Zhao, G.C., 2009. Metamorphic evolution of major tectonic units in the basement of the North China Craton: Key issues and discussion. Acta Petrol. Sin. 25, 1772–1792 (in Chinese with English abstract).
Zhao, G.C., Zhai, M., 2013. Lithotectonic elements of Precambrian basement in the North China Craton: Review and tectonic implications. Gondwana Res. 23, 1207–1240.
Zhao, G.C., Simon, A.W., Cawood, P.A., 1998. Thermal evolution of Archean basement rocks from the eastern part of the North China Craton and its bearing on tectonic setting. International Geological Review 40, 706–721.
Zhao, G.C., Simon, A.W., Cawood, P.A., Lu, L.Z., 1999. Tectonothermal history of the basement rocks in the western zone of the North China Craton and its tectonic implications. Tectonophysics 310, 37–53.
Zhao, G.C., Cawood, P.A., Simon, A.W., Sun, M., Lu, L.Z., 2000. Metamorphism of basement rocks in the central zone of the North China Craton: implication for Palaeoproterozoic tectonic evolution. Precambrian Res. 103, 55–88.
Zhao, G.C., Cawood, P.A., Simon, A.W., Lu, L.Z., 2001a. High-pressure granulite (retrograded eclogites) from the Hengshan Complex, North China Craton: petrology and tectonic implications. J. Petrol. 42, 1141–1170.
Zhao, G.C., Simon, A.W., Cawood, P.A., Sun, M., 2001b. Archean blocks and their boundaries in the North China Craton: lithological, geochemical, structural and P-T path constrains and tectonic evolution. Precambrian Res. 107, 45–73.
Zhao, G.C., Simon, A.W., Cawood, P.A., Sun, M., 2002a. SHRIMP U-Pb zircon ages of the Fuping Complex: implications for late Achaean to Paleoproterozoic accretion and assembly of the North China Craton. Am. J. Sci. 302, 191–226.
Zhao, G.C., Cawood, P.A., Wilde, S.A., Sun, M., 2002b. Review of global 2.1–1.8 Ga orogens: implications for a pre-Rodinia supercontinent. Earth Sci. Rev. 59, 125–162.
Zhao, G.C., Sun, M., Simon, A.W., 2003. Correlations between the Eastern Block of the North China Craton and the South Indian Block of the Indian Shield: a pre-Rodinia North China-India link. Precambrian Res. 122, 201–233.
Zhao, G.C., Sun, M., Wilde, S.A., Li, S.Z., 2004. A Paleo-Mesoproterozoic supercontinent: assembly, growth and breakup. Earth Sci. Rev. 67, 91–123.
Zhao, G.C., Sun, M., Simon, Wilde, Li, S.Z., 2005. Late Archean to Paleoproterozoic evolution of the North China Craton: key issues revisited. Precambrian Res. 136, 177–202.
Zhao, G.C., Sun, M., Wilde, S., Li, S.Z., Liu, S.W., Zhang, J., 2006a. Composite nature of the North China Granulite-Facies Belt: Tectonothermal and geochronological constraints. Gondwana Res. 9, 337–348.
Zhao, G.C., Cao, L., Wilde, S.A., Sun, M., Choe, W.J., Li, S.Z., 2006b. Implications based on the first SHRIMP U-Pb zircon dating on Precambrian granitoid rocks in North Korea. Earth Planet. Sci. Lett. 251, 365–379.
Zhao, G.C., Yin, C.Q., Guo, J.H., Sun, M., Li, S.Z., Li, X.P., Wu, C.M., Liu, C.H., 2010. Metamorphism of the Luliang amphibolite: implications for the tectonic evolution of the North China Craton. Am. J. Sci. 310, 1480–1502.
Zhao, G.C., Li, S.Z., Sun, M., Wilde, S.A., 2011. Assembly, accretion, and break-up of the Palaeo-Mesoproterozoic Columbia supercontinent: records in the North China Craton revisited. Int. Geol. Rev. 53, 1331–1356.
Zhao, G.C., Cawood, P.A., Li, S.Z., Wilde, S.A., Sun, M., Zhang, J., He, Y.H., Yin, C.Q., 2012. Amalgamation of the North China Craton: Key issues and discussion. Precambrian Res. 222–223, 55–76.
Zhao, J.X., McCulloch, M.T., 1995. Geochemical and Nd isotopic systematics of granites from the Arunta Inlier, central Australia: implications for Proterozoic crustal evolution. Precambrian Res. 71, 265–299.
Zhou, J.B., Wilde, S.A., Zhao, G.C., Zheng, C.Q., Jin, W., Zhang, X.Z., Cheng, H., 2008b. SHRIMP U–Pb zircon dating of the Neoproterozoic Penglai Group and Archean gneisses from the Jiaobei Terrane, North China Craton, and their tectonic implications. Precambrian Res. 160, 323–340.
Zhou, X.W., Dong, Y.S., Wei, C.D., 2001. The genesis and evolution of the metamorphic minerals of Khondalite series in Nanshu district of Shandong Province. Journal of Changchun University of Sciences and Technology 31, 116–121 (in Chinese with English abstract).
Zhou, X.W., Wei, C.J., Dong, Y.S., Lu, L.Z., 2003. Characteristics of diffusion zoning in garnet and implications for genesis from Al-rich rock series of the Jingshan group in north Jiaodong. Acta Petrol. Sin. 19, 752–760 (in Chinese with English abstract).
Zhou, X.W., Wei, C.J., Geng, Y.S., Zheng, L.F., 2004. Discovery and implications of the high-pressure pelitic granulites from the Jiaobei massif. Chin. Sci. Bull. 49, 1942–1948 (in Chinese with English abstract).
Zhou, X.W., Wei, C.J., Geng, Y.S., Zhang, L.F., 2005. Electron microprobe monazite Th-Pb dating and its constraints on multi-stage metamorphism of low-pressure pelitic granulite from the Jingshan Group in the Jiaobei massif. Chin. Sci. Bull. 50, 1009–1015 (in Chinese with English abstract).
Zhou, X.W., Wei, C.J., Zhang, S.K., 2006. Implications of micro-compositions of garnet and biotite from high-grade meta-pelites. Prog. Nat. Sci. 16, 209–214.
Zhou, X.W., Wei, C.J., Geng, Y.S., 2007. Phase equilibria P-T path of the high- and low-pressure pelitic granulites from the Jiaobei massif. Earth Science Frontiers 14 (1), 135–143 (in Chinese with English abstract).
Zhou, X.W., Zhao, G.C., Wei, C.J., Geng, Y.S., Sun, M., 2008a. EPMA U–Pb monazite and Shrimp U–Pb zircon Geochronology of high-pressure pelitic granulites in the Jiaobei massif of the North China Craton. Am. J. Sci. 308, 328–350.